

# Spontaneous Chern-Euler Duality Transitions

Kang Yang,<sup>1</sup> Zhi Li,<sup>2</sup> Peng Xue,<sup>3</sup> Emil J. Bergholtz,<sup>4</sup> and Piet W. Brouwer<sup>1</sup>

<sup>1</sup>*Dahlem Center for Complex Quantum Systems and Fachbereich Physik, Freie Universität Berlin, 14195 Berlin, Germany*

<sup>2</sup>*Perimeter Institute for Theoretical Physics, Waterloo, Ontario N2L 2Y5, Canada*

<sup>3</sup>*Beijing Computational Science Research Center, Beijing 100193, China*

<sup>4</sup>*Department of Physics, Stockholm University, AlbaNova University Center, 106 91 Stockholm, Sweden*

(Dated: March 31, 2025)

Topological phase transitions are typically characterized by abrupt changes in a quantized invariant. Here we report a contrasting paradigm in non-Hermitian parity-time symmetric systems, where the topological invariant remains conserved, but its nature transitions between the Chern number, characteristic of chiral transport in complex bands, and the Euler number, which characterizes the number of nodal points in pairs of real bands. The transition features qualitative changes in the non-Abelian geometric phases during spontaneous parity-time symmetry breaking, where different quantized components become mutually convertible. Our findings establish a novel topological duality principle governing transitions across symmetry classes and reveal unique non-unitary features intertwining topology, symmetry, and non-Abelian gauge structure.

## INTRODUCTION

Symmetry, geometry, and topology play fundamental roles in modern physics, from elementary particles and gravity to quantum materials. Knowledge of the global topology of energy bands in quantum materials provides insights into the nature of the quantum states and gives rise to precisely quantized observables [1]. The best known example of such a topological invariant is the Chern number, which describes the topology of complex vector bundles in two dimensions. The topological robustness of the Chern number underpins one of the most precisely measured physical constants, the Hall conductance in the quantum Hall effect. A transition between different quantized values requires the closing of a band gap, accompanied by the appearance of Dirac or Weyl points [2].

The advent of dissipative photonic or acoustic systems with parity-time (PT) symmetry has expanded the scope of topological physics [3–7]. PT-symmetric band structures are described by a real-valued “Hamiltonian” matrix  $H(\mathbf{k})$ , which is not symmetric in the presence of loss and gain [8]. Eigenstates and eigenvalues of  $H(\mathbf{k})$  are either real or appear in complex-conjugated pairs [9]. In the latter case, the PT symmetry of  $H(\mathbf{k})$  is spontaneously broken at the level of the eigenvalues and eigenstates. Transitions between PT-symmetric and PT-broken eigenstates take place at exceptional points (EPs) in the spectrum of  $H(\mathbf{k})$ , at which two real eigenvalues of  $H(\mathbf{k})$  meet and convert into a pair of complex-conjugate eigenvalues [10–18].

From a topological perspective, real and complex bands of eigenstates are sharply different: Complex bands exhibit chiral transport described by a Chern number, whereas the bands associated with real eigenstates always have a vanishing Chern number and chiral transport is ruled out. On the other side, a pair of real bands may have nonchiral topology described by the integer-valued Euler number [19–21]. A nonzero Euler number signals an obstruction for opening a gap between the two bands [19, 20, 22]. The possibility to realize two different topological paradigms in the same physical system [23] sets non-Hermitian PT-symmetric systems apart from their counterparts without symmetries [24–

28] as well as Hermitian systems. In this work, we show that PT-symmetric systems admit a direct transition between real and complex bands, which follows a Chern-Euler duality principle and takes place without additional gap closings. We analyze this *spontaneous Chern-Euler duality transition* and show how the real and complex topologies at the two ends of the transition are related.

To make the Chern-Euler duality transition explicit, we compare transitions between three PT-symmetric  $3 \times 3$  band structures: (i) A Hermitian model  $H_{\text{Euler}}(\mathbf{k})$ , for which the lowest two bands are separated from the third band by a gap and have nontrivial topology with Euler number  $|\chi| = 2$ , (ii) a non-Hermitian band structure  $H_{\text{Chern}}(\mathbf{k})$ , which has two complex-conjugate complex bands with Chern number  $C_{\pm} = \pm 2$  and one real band, and (iii) a Hermitian trivial model  $H_{\text{trivial}}(\mathbf{k})$ , which has three trivial bands separated by band gaps. Complex spectra corresponding to these models and their transitions are shown schematically in Fig. 1.

The real-to-complex transition between  $H_{\text{Euler}}(\mathbf{k})$  and  $H_{\text{Chern}}(\mathbf{k})$  takes place via spontaneous PT symmetry breaking. It starts with the formation of EPs in the lowest two bands, which form an “exceptional ring” (ER) in reciprocal space [29, 30]. In the course of the transition, the ER sweeps over the Brillouin zone (BZ), so that eventually all eigenvalues and eigenstates in the initial two Euler bands become complex and an imaginary spectral gap opens up. The two real bands evolve into two complex bands without connecting to any other bands; the gap to the third (real) band remains open at all times. We prove that in general such a “dual transition” of a pair of bands can take place *if and only if* the absolute value of the Chern number of the complex band pair equals the absolute value of the Euler number of the real band pair,

$$|C_{\pm}| = |\chi|. \quad (1)$$

Bands satisfying this condition, such as our choice of  $H_{\text{Euler}}(\mathbf{k})$  and  $H_{\text{Chern}}(\mathbf{k})$ , physically realize the duality relation between Chern classes and Euler classes in vector bundle theories [31]. If the condition (1) is not met, a spontaneous PT-breaking transition involving only two bands is impossible. Instead, all three bands must connect during the transition. Such a “non-dual” transition may involve a

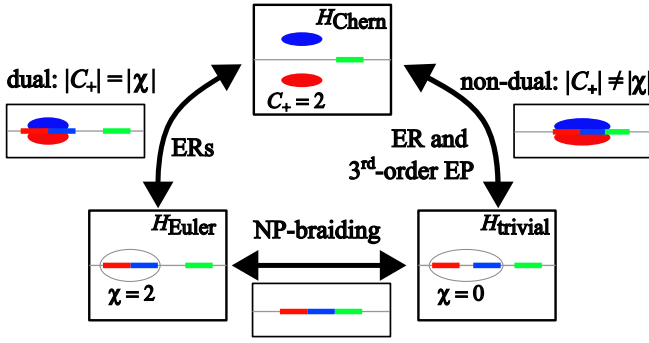


FIG. 1. Schematics of the transitions studied in this article. The boxes schematically indicate the spectra at the three types of models  $H_{\text{Euler}}$ ,  $H_{\text{Chern}}$ , and  $H_{\text{trivial}}$  and during the transitions between them. The Chern-Euler duality transition between bands 1 and 2 (shown in red and blue) takes place without involvement of the third, real band (green). The non-dual transition between bands with different Chern number and Euler number forces connection between all three bands. In the Hermitian regime, the Euler topology stably protects the nodal points (NPs) between the bands 1 and 2.

third-order EP, as we observe for the transition  $H_{\text{trivial}}(\mathbf{k}) \rightarrow H_{\text{Chern}}(\mathbf{k})$ . The non-dual transition generalizes the Hermitian limit transition  $H_{\text{trivial}}(\mathbf{k}) \rightarrow H_{\text{Euler}}(\mathbf{k})$ , which proceeds via the braiding of nodal points (NPs) connecting pairs of bands [19, 20, 32], see Fig. 1.

The Chern-Euler duality transition provides a universal mechanism to generate Chern bands by spontaneously breaking the PT symmetry in Euler bands via loss. The topological duality paves the way for engineering topological states in PT-symmetric systems.

### HERMITIAN AND NON-HERMITIAN PT-SYMMETRIC MODELS

The PT-symmetric three-band models we consider are described by a three-component vector  $|\psi(t, \mathbf{k})\rangle$ , which evolves according to the Schrödinger-like equation  $i\partial_t|\psi(t, \mathbf{k})\rangle = H(\mathbf{k})|\psi(t, \mathbf{k})\rangle$ , where  $H(\mathbf{k})$  is a real  $3 \times 3$  matrix, as required by PT symmetry. The two variables  $\mathbf{k} = (k_x, k_y)$ , which may be quasi-momenta of photons or tuning parameters of the system [3–6], reside in a torus, thus forming an effective BZ. The eigenvalues  $\omega_j(\mathbf{k})$  ( $j = 1, 2, 3$ ), of  $H(\mathbf{k})$  form three energy bands, which may be complex if  $H(\mathbf{k})$  is non-Hermitian. Three bands is the minimal requirement for a non-vanishing Euler topology in the Hermitian regime. (The Euler number of a  $2 \times 2$  model is always trivial.)

We first summarize the relevant properties of the three reference band structures  $H_{\text{Euler}}(\mathbf{k})$ ,  $H_{\text{Chern}}(\mathbf{k})$ , and  $H_{\text{trivial}}(\mathbf{k})$ . Explicit expressions are given in the Methods Section. For the Hermitian models  $H_{\text{Euler}}(\mathbf{k})$  and  $H_{\text{trivial}}(\mathbf{k})$ , all three eigenvalues and eigenstates are real. Both models have a spectral gap between the middle and upper band. We label the eigenvalues as  $\omega_1(\mathbf{k}) \leq \omega_2(\mathbf{k}) < \omega_3(\mathbf{k})$ . For  $H_{\text{trivial}}(\mathbf{k})$  there is also a spectral gap between bands 1 and 2, and all three bands are topologically trivial. For  $H_{\text{Euler}}(\mathbf{k})$ ,

the topology of the combined bands 1 and 2 is described by the Euler number  $|\chi| = 2$ . (The Euler number must be an even integer for a three-band model [19, 20].) A nonzero Euler number  $\chi \neq 0$  protects  $2|\chi|$  nodal points (NPs) [19, 20, 22] at which bands 1 and 2 touch.

The Euler number  $\chi$  can be calculated from the non-Abelian Berry curvature  $B(\mathbf{k})$ , a  $2 \times 2$  matrix generalizing the Berry curvature to a pair of bands [33],

$$B(\mathbf{k}) = \partial_{k_x} A_y(\mathbf{k}) - \partial_{k_y} A_x(\mathbf{k}) - i[A_x(\mathbf{k}), A_y(\mathbf{k})]. \quad (2)$$

Here  $A_{x/y}(\mathbf{k})_{ij} = i\langle\psi_i(\mathbf{k})|\partial_{k_{x/y}}\psi_j(\mathbf{k})\rangle$  is the non-Abelian Berry connection, matrix indices  $i, j \in \{1, 2\}$  correspond to bands indices, and  $[\cdot, \cdot]$  denotes the commutator. If  $H(\mathbf{k})$  is Hermitian,  $B(\mathbf{k})$  is an antisymmetric  $2 \times 2$  matrix and  $\chi$  is given by the integral of the off-diagonal component  $B_{12}(\mathbf{k})$  over the BZ [20, 34],

$$\chi = \frac{1}{2\pi i} \int B_{12}(\mathbf{k}) d^2k. \quad (3)$$

The expression also works for non-Hermitian real bands after applying an orthonormalization as described in the Methods Section. The Euler number has a sign ambiguity related to the choice of the orientation in the eigenstate basis  $|\psi_{1,2}(\mathbf{k})\rangle$ , which is why only its absolute value  $|\chi|$  appear in physical expressions.

The different topology of the two Hermitian models  $H_{\text{trivial}}(\mathbf{k})$  and  $H_{\text{Euler}}(\mathbf{k})$  is reflected in the continuous transition between these models, which has been previously studied in the literature [19, 20, 22, 32]. The nonzero Euler number obstructs a direct gap opening between bands 1 and 2 of  $H_{\text{Euler}}(\mathbf{k})$  [19, 20, 22, 32]. Instead, the gap opening between these two bands requires a closing of the gap with the third band first. After this gap closing, NPs connecting bands 2 and 3 appear. Winding of these “2-3 nodes” relative to the “1-2 nodes” between bands 1 and 2 changes the topology of the latter [19, 20, 32], allowing for the opening of a gap between bands 1 and 2 after the Euler topology is trivialized.

In the remainder of this article, we focus on transitions involving the non-Hermitian model  $H_{\text{Chern}}$ , which has two complex bands that are complex conjugates of each other, and one real band. The complex bands are separated by an *imaginary* spectral gap, indicating a complete spontaneous PT-symmetry breaking [9]. We use  $|\psi_+(\mathbf{k})\rangle$  to represent the complex eigenstate with eigenvalue  $\omega(\mathbf{k})$  on the lower half complex plane, and  $|\psi_-(\mathbf{k})\rangle \equiv |\psi_+(\mathbf{k})\rangle^*$  to represent the conjugate partner with eigenvalue  $\omega^*(\mathbf{k})$ . The topology of the complex bands is characterized by the Chern number  $C_+ = -C_-$  [23], which is the integral of the diagonal Berry curvature  $B_{jj}(\mathbf{k})$  associated with one of the complex bands over the BZ ( $j \in \{+, -\}$ ),

$$C_j = \frac{1}{2\pi} \int B_{jj}(\mathbf{k}) d^2k. \quad (4)$$

### CHERN-EULER DUALITY TRANSITION

To analyze the Chern-Euler duality transition, we consider interpolations  $H_\lambda(\mathbf{k})$  between  $H_{\text{Euler}}(\mathbf{k})$  and  $H_{\text{Chern}}(\mathbf{k})$ ,  $0 \leq$

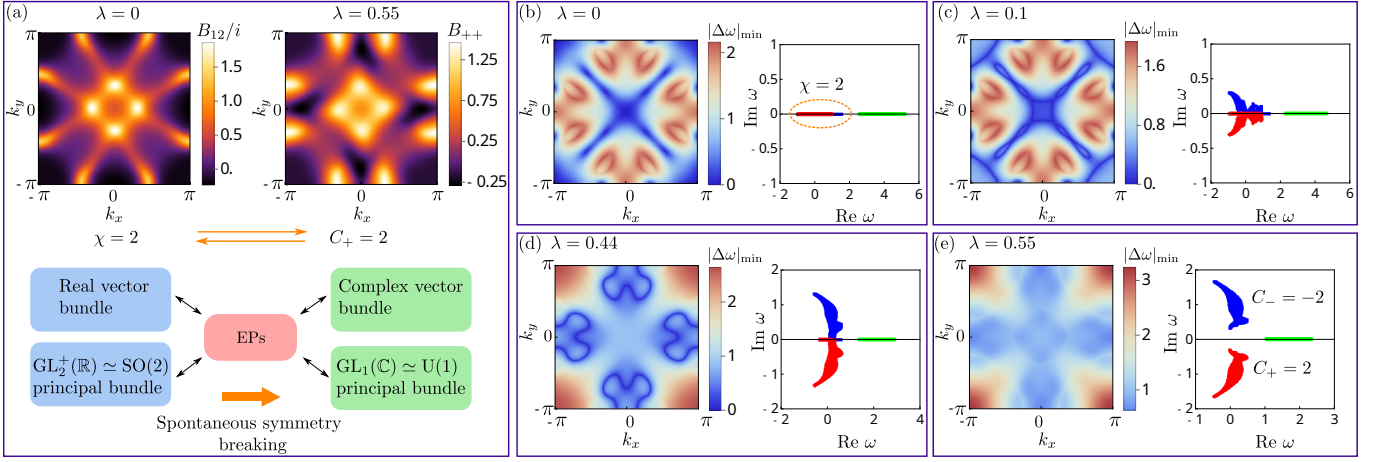


**FIG. 2. The spontaneous Chern-Euler duality transition.** (a) Top: The off-diagonal Berry curvature  $B_{12}$  at  $\lambda = 0$  (left) and the diagonal Berry curvature  $B_{++}$  at  $\lambda = 0.55$  (right) over the two-dimensional BZ. Their integrals are equal to  $\chi = 2$  and  $C_+ = 2$ , respectively. Bottom: In the symmetry-preserving regime, the paired eigenstates are described by a real rank-two vector bundle, whose frame bundle is a  $\text{GL}_2^+(\mathbb{R})$  bundle. After spontaneous symmetry breaking, the eigenstates are described by two complex rank-one vector bundles, whose frames form two  $\text{GL}_1(\mathbb{C})$  bundles. The  $\text{GL}_2^+(\mathbb{R})$  topology is continuously related to the  $\text{GL}_1(\mathbb{C})$  topology, leading to the conservation  $|\chi| = |C_{\pm}|$ . (b)–(e) The minimum of the local eigenvalue gaps  $|\Delta\omega(\mathbf{k})|_{\min} \equiv \text{Min}_{i,j} |\omega_i(\mathbf{k}) - \omega_j(\mathbf{k})|$  of  $H_{\lambda}$  at  $\lambda = 0.1$  (b),  $\lambda = 0.44$  (c), and  $\lambda = 0.55$ , reflecting the shapes of level crossings in the BZ. The corresponding complex spectra are shown in the right panel of each figure, with the three bands labeled by different colors.

$\lambda \leq 1$ ,

$$H_{\lambda}(\mathbf{k}) = (1 - \lambda)H_{\text{Euler}}(\mathbf{k}) + \lambda H_{\text{Chern}}(\mathbf{k}). \quad (5)$$

Figure 2a compares the off-diagonal Berry curvature  $B_{12}(\mathbf{k})$  in the Hermitian limit  $\lambda = 0$  with the diagonal Berry curvature  $B_{++}(\mathbf{k})$  for  $\lambda = 0.55$ , where the PT symmetry is spontaneously broken in the entire BZ. Initially at  $\lambda = 0$ , the integral of the off-diagonal Berry curvature  $B_{12}(\mathbf{k})$  takes the quantized value  $\chi = 2$ . In the fully PT-broken case at  $\lambda = 0.55$ , the integral of the diagonal Berry curvature  $B_{++}(\mathbf{k})$  of the complex band is  $C_+ = 2$  ( $C_- = -2$  due to the PT symmetry). The transition from  $H_{\text{Euler}}(\mathbf{k})$  to  $H_{\text{Chern}}(\mathbf{k})$  takes place through the formation of ERs. As  $\lambda$  increases, these ERs grow out of the NPs of  $H_{\text{Euler}}(\mathbf{k})$ , then sweep over the BZ, see Figs. 2b–d, until all eigenvalues of bands 1 and 2 have gone through the real-to-complex transition and an imaginary spectral gap is opened between the resulting two complex bands (Fig. 2e). A key observation is that the real band 3 remains detached from bands 1 and 2 at all times during the spontaneous PT-breaking transition, as shown in Fig. 2b–e. The opening of an imaginary gap between bands 1 and 2 without intermediate gap closings to any other band is special to the non-Hermitian regime, as the nontrivial Euler-number topology of the bands 1 and 2 prevents the opening of a real gap between them in the Hermitian limit ([22] and Supplemental Material).

In the spontaneous PT-symmetry breaking transition, the topology of the real Euler bands 1 and 2, which have Euler number  $|\chi| = 2$ , is passed on to the that of the complex Chern bands, which have Chern number  $C_{\pm} = \pm 2$ . In this sense, the Chern bands in the PT-breaking regime are *dual* to the pair of Euler bands in the PT-symmetry preserving regime. Such duality also holds for bands with Euler numbers and Chern numbers other than two: *Spontaneous PT-breaking transitions*

*without involvement of remote bands can occur only between Euler and Chern bands with  $|\chi| = |C_{\pm}|$*  (Eq. (1)). This duality condition is the main result of this article. It also holds for systems with more than three bands and equally applies to the reverse transition: if a pair of bands transit from the PT-broken regime to the PT-symmetric regime by closing their imaginary gap, they will carry an Euler number  $\chi$  dictated by their initial Chern numbers  $C_+ = -C_-$  if they do not touch any other bands in the process. A direct consequence is that two-band models cannot host Chern bands after spontaneously breaking PT-symmetry [23, 35], since the real band pair in a two-band model always have  $\chi = 0$ .

The outline of a proof of the Chern-Euler duality relation is given in the Methods Section; for a complete proof we refer to the Supplemental Material, where we examine the PT-breaking transition from multiple mathematical perspectives. The real Euler bands have a gauge structure of  $\text{GL}_2^+(\mathbb{R})$  in the non-Hermitian regime, generalizing the  $\text{SO}(2)$  gauge structure of the Hermitian case, while the paired Chern bands have a  $\text{GL}_1(\mathbb{C})$  gauge structure [23], see Fig. 2a. These two gauge groups are homotopy equivalent, as shown in Supplemental Material S3, which means that they share the same global topology. The Chern-Euler duality reflects the continuity of the gauge-structure topology across ERs throughout the PT-breaking transition, as we discuss in more detail in Methods and supplementary material S5. Geometrically, the states in the PT-preserving regime are described by real vector bundles, while those in the PT-breaking regime are described by complex vector bundles. These different types of vector bundles are related to each other by realification and complexification operations [34]. In Supplemental Material S4 we provide a geometric proof of the Chern-Euler duality by demonstrating a series of isomorphisms in the realification and complexifi-

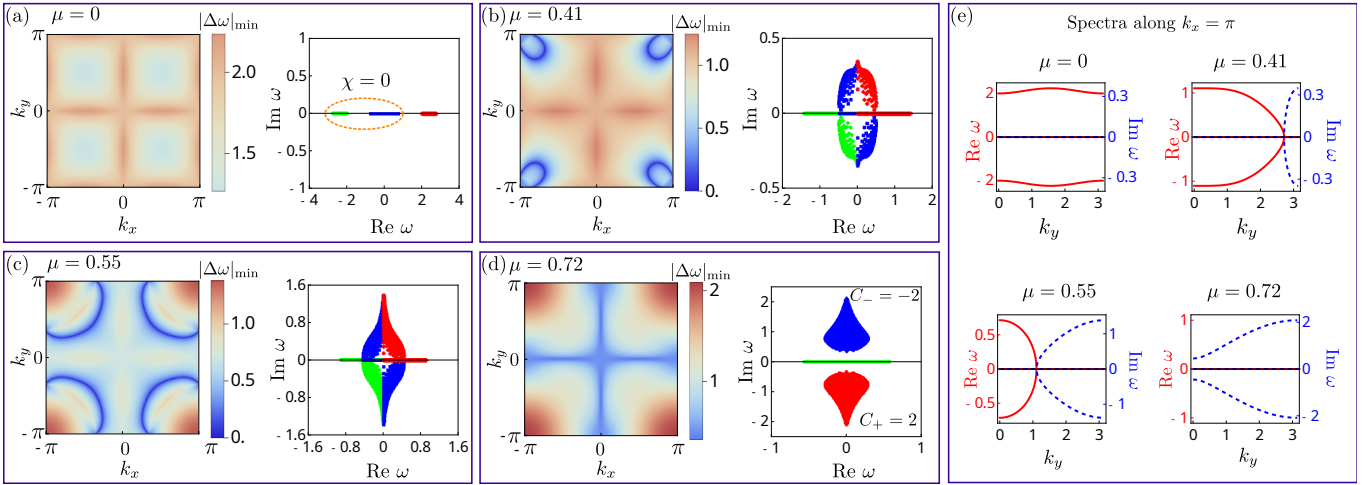


FIG. 3. **The non-dual transition from trivial bands to Chern bands.** (a)-(d). The minimum eigenvalue gap  $|\Delta\omega(\mathbf{k})|_{\min} = \text{Min}_{i,j} |\omega_i(\mathbf{k}) - \omega_j(\mathbf{k})|$  and the spectra of  $H_\mu$  on the complex plane at  $\mu = 0$  in (a),  $\mu = 0.41$  in (b),  $\mu = 0.55$  in (c), and  $\mu = 0.72$  in (d). All the three bands are connected together during the non-dual transition. (e) The real and imaginary parts of the spectra as a function of  $k_y$  at fixed  $k_x = \pi$  for different  $\mu$ . Triple level crossings, i.e., EP3s are generated during this non-dual transition.

cation of the corresponding Bloch bundles.

### NON-DUAL TRANSITION

We contrast the Chern-Euler duality transition with the transition  $H_{\text{trivial}}(\mathbf{k}) \rightarrow H_{\text{Chern}}(\mathbf{k})$ , which is a spontaneous PT-breaking transition involving bands that violate Eq. (1). We consider the interpolating Hamiltonians

$$H_\mu(\mathbf{k}) = (1 - \mu)H_{\text{trivial}}(\mathbf{k}) + \mu H_{\text{Chern}}(\mathbf{k}). \quad (6)$$

Spectra of  $H_\mu(\mathbf{k})$  at various stages in the transition are shown in Fig. 3a-d. As the real bands in the initial model  $H_{\text{trivial}}(\mathbf{k})$  carry  $\chi = 0$ , the transition to the complex Chern bands of  $H_{\text{Chern}}(\mathbf{k})$  can only take place after all three bands cross simultaneously. The eigenvalues in Fig. 3b and c indicate the emergence of ERs. These ERs are connecting different pair of bands and terminate at third-order EPs (Fig. 3e), where all three bands touch and join together through level crossings. The ERs expand and progressively sweep across the BZ as  $\mu$  is increased further to 0.55. The transition is complete at  $\mu = 0.72$ , as shown in Figs. 3d, where two imaginary gaps to bands with Chern number  $C_\pm = \pm 2$  are opened symmetrically around the real axis. The occurrence of a triple band touching during the non-dual transition provides fresh insights on higher-order EPs [14–18] in PT-symmetric systems.

### DISCUSSION

In this article, we extended the concept of topological transitions to the realm of topological duality. The spontaneous PT-symmetry breaking in non-Hermitian PT-symmetric systems corresponds to the natural duality between complex vector bundles and real vector bundles. As a result, the same

topology manifests as two distinct quantized properties, depending on the symmetry regime. Dissipative photonic and acoustic systems give this paradigm in vector bundle theory a concrete physical context.

Experimentally measurable geometric phases and level crossings in PT-symmetric models are diagnoses of the dual and non-dual transitions. The shapes of exceptional rings and the appearance of triple band crossings can be probed in a wide range of platforms [3–6, 26–30]. Due to the imaginary spectral gap, at a given  $\mathbf{k}$  any initial state will evolve into the Chern band  $|\psi_-(\mathbf{k})\rangle$  after dynamic evolution. Berry curvatures are geometric phases around small plaquettes in the  $\mathbf{k}$ -space [36]. They can be measured by interferometry between the final states  $|\psi_-(\mathbf{k})\rangle$  and  $|\psi_-(\mathbf{k} + \delta\mathbf{k})\rangle$  at different parameters of  $\mathbf{k}$  [37].

In addition to the spectral phenomena presented here, there are many other phenomena related to the topological bands, including in-gap edge modes and Wannierization. It will be interesting to investigate these properties during the duality transition. In three-level models, which have been used to illustrate the Chern-Euler transition in this article, Chern numbers and Euler numbers can only take even values [23, 38]. The detailed investigation of a system with more bands, where the topological invariants can be arbitrary integers and Chern bands can coexist with Euler bands, is left for future work.

**Acknowledgements.** The authors thank Vatsal Dwivedi and Felix von Oppen for fruitful discussions. KY is supported by the ANR-DFG project (TWISTGRAPH). ZL is supported by Perimeter Institute; research at Perimeter Institute is supported in part by the Government of Canada through the Department of Innovation, Science and Economic Development and by the Province of Ontario through the Ministry of Colleges and Universities. PX is supported by the National Key R&D Program of China (Grant No. 2023YFA1406701) and National Natural Science Foundation of China (Grants No. 12025401, No. 92265209). EJB is supported by the

- 
- [1] F. D. M. Haldane, Nobel lecture: Topological quantum matter, *Rev. Mod. Phys.* **89**, 040502 (2017).
- [2] N. P. Armitage, E. J. Mele, and A. Vishwanath, Weyl and Dirac semimetals in three-dimensional solids, *Rev. Mod. Phys.* **90**, 015001 (2018).
- [3] M.-A. Miri and A. Alù, Exceptional points in optics and photonics, *Science* **363**, 7709 (2019).
- [4] L. Feng, R. El-Ganainy, and L. Ge, Non-Hermitian photonics based on parity–time symmetry, *Nat. Photon.* **11**, 752 (2017).
- [5] R. El-Ganainy, K. G. Makris, M. Khajavikhan, Z. H. Muslimani, S. Rotter, and D. N. Christodoulides, Non-Hermitian physics and  $\mathcal{PT}$  symmetry, *Nat. Phys.* **14**, 11 (2018).
- [6] Ş. K. Özdemir, S. Rotter, F. Nori, and L. Yang, Parity–time symmetry and exceptional points in photonics, *Nat. Mat.* **18**, 783 (2019).
- [7] E. J. Bergholtz, J. C. Budich, and F. K. Kunst, Exceptional topology of non-hermitian systems, *Rev. Mod. Phys.* **93**, 015005 (2021).
- [8] C. M. Bender and D. W. Hook,  $\mathcal{PT}$ -symmetric quantum mechanics, *Rev. Mod. Phys.* **96**, 045002 (2024).
- [9] C. M. Bender, Making sense of non-Hermitian Hamiltonians, *Rep. Prog. Phys.* **70**, 947 (2007).
- [10] T. Kato, *Perturbation theory for linear operators*, Vol. 132 (Springer Science & Business Media, 2013).
- [11] A. Guo, G. J. Salamo, D. Duchesne, R. Morandotti, M. Volatier-Ravat, V. Aimez, G. A. Siviloglou, and D. N. Christodoulides, Observation of  $\mathcal{PT}$ -symmetry breaking in complex optical potentials, *Phys. Rev. Lett.* **103**, 093902 (2009).
- [12] C. E. Rüter, K. G. Makris, R. El-Ganainy, D. N. Christodoulides, M. Segev, and D. Kip, Observation of parity–time symmetry in optics, *Nat. Phys.* **6**, 192 (2010).
- [13] Y. D. Chong, L. Ge, and A. D. Stone,  $\mathcal{PT}$ -symmetry breaking and laser-absorber modes in optical scattering systems, *Phys. Rev. Lett.* **106**, 093902 (2011).
- [14] H. Hodaei, A. U. Hassan, S. Wittek, H. Garcia-Gracia, R. El-Ganainy, D. N. Christodoulides, and M. Khajavikhan, Enhanced sensitivity at higher-order exceptional points, *Nature* **548**, 187 (2017).
- [15] Z. Xiao, H. Li, T. Kottos, and A. Alù, Enhanced sensing and nondegraded thermal noise performance based on  $\mathcal{PT}$ -symmetric electronic circuits with a sixth-order exceptional point, *Phys. Rev. Lett.* **123**, 213901 (2019).
- [16] W. Tang, X. Jiang, K. Ding, Y.-X. Xiao, Z.-Q. Zhang, C. T. Chan, and G. Ma, Exceptional nexus with a hybrid topological invariant, *Science* **370**, 1077 (2020).
- [17] P. Delplace, T. Yoshida, and Y. Hatsugai, Symmetry-protected multifold exceptional points and their topological characterization, *Phys. Rev. Lett.* **127**, 186602 (2021).
- [18] I. Mandal and E. J. Bergholtz, Symmetry and higher-order exceptional points, *Phys. Rev. Lett.* **127**, 186601 (2021).
- [19] J. Ahn, S. Park, and B.-J. Yang, Failure of Nielsen-Ninomiya theorem and fragile topology in two-dimensional systems with space-time inversion symmetry: Application to twisted bilayer graphene at magic angle, *Phys. Rev. X* **9**, 021013 (2019).
- [20] A. Bouhon, Q. Wu, R.-J. Slager, H. Weng, O. V. Yazyev, and T. Bzdušek, Non-Abelian reciprocal braiding of weyl points and its manifestation in ZrTe, *Nat. Phys.* **16**, 1137 (2020).
- [21] K. Wang, J.-X. Dai, L. B. Shao, S. A. Yang, and Y. X. Zhao, Boundary criticality of  $\mathcal{PT}$ -invariant topology and second-order nodal-line semimetals, *Phys. Rev. Lett.* **125**, 126403 (2020).
- [22] F. N. Ünal, A. Bouhon, and R.-J. Slager, Topological Euler class as a dynamical observable in optical lattices, *Phys. Rev. Lett.* **125**, 053601 (2020).
- [23] K. Yang, Z. Li, J. L. K. König, L. Røddland, M. Stålhammar, and E. J. Bergholtz, Homotopy, symmetry, and non-Hermitian band topology, *Rep. Prog. Phys.* **87**, 078002 (2024).
- [24] C. C. Wojcik, X.-Q. Sun, T. Bzdušek, and S. Fan, Homotopy characterization of non-Hermitian Hamiltonians, *Phys. Rev. B* **101**, 205417 (2020).
- [25] Z. Li and R. S. K. Mong, Homotopical characterization of non-Hermitian band structures, *Phys. Rev. B* **103**, 155129 (2021).
- [26] K. Wang, A. Dutt, C. C. Wojcik, and S. Fan, Topological complex-energy braiding of non-Hermitian bands, *Nature* **598**, 59 (2021).
- [27] Y. S. Patil, J. Höller, P. A. Henry, C. Guria, Y. Zhang, L. Jiang, N. Kralj, N. Read, and J. G. Harris, Measuring the knot of non-Hermitian degeneracies and non-commuting braids, *Nature* **607**, 271 (2022).
- [28] K. Ding, C. Fang, and G. Ma, Non-Hermitian topology and exceptional-point geometries, *Nat. Rev. Phys.* **4**, 745 (2022).
- [29] B. Zhen, C. W. Hsu, Y. Igarashi, L. Lu, I. Kaminer, A. Pick, S.-L. Chua, J. D. Joannopoulos, and M. Soljačić, Spawning rings of exceptional points out of Dirac cones, *Nature* **525**, 354 (2015).
- [30] A. Cerjan, S. Huang, M. Wang, K. P. Chen, Y. Chong, and M. C. Rechtsman, Experimental realization of a Weyl exceptional ring, *Nat. Photon.* **13**, 623 (2019).
- [31] R. Bott, L. W. Tu, *et al.*, *Differential forms in algebraic topology*, Vol. 82 (Springer New York, NY, 1982).
- [32] Q. Wu, A. A. Soluyanov, and T. Bzdušek, Non-Abelian band topology in noninteracting metals, *Science* **365**, 1273 (2019).
- [33] F. Wilczek and A. Zee, Appearance of gauge structure in simple dynamical systems, *Phys. Rev. Lett.* **52**, 2111 (1984).
- [34] J. Milnor and J. Stasheff, *Characteristic Classes*, Annals of mathematics studies (Princeton University Press, 1974).
- [35] Y. C. Hu and T. L. Hughes, Absence of topological insulator phases in non-Hermitian  $\mathcal{PT}$ -symmetric Hamiltonians, *Phys. Rev. B* **84**, 153101 (2011).
- [36] T. Fukui, Y. Hatsugai, and H. Suzuki, Chern numbers in discretized Brillouin zone: Efficient method of computing (spin) Hall conductances, *J. Phys. Soc. Jpn.* **74**, 1674 (2005).
- [37] K. Wang, J. L. K. König, K. Yang, L. Xiao, W. Yi, E. J. Bergholtz, and P. Xue, Photonic non-abelian braid monopole, *arXiv preprint arXiv:2410.08191* (2024).
- [38] P. W. Brouwer and V. Dwivedi, Homotopic classification of band structures: Stable, fragile, delicate, and stable representation-protected topology, *Phys. Rev. B* **108**, 155137 (2023).
- [39] Y. Zhao, Equivariant  $\mathcal{PT}$ -symmetric real Chern insulators, *Front. Phys.* **15**, 1 (2020).
- [40] E. M. Graefe, U. Günther, H. J. Korsch, and A. E. Niederle, A non-Hermitian  $\mathcal{PT}$  symmetric Bose–Hubbard model: eigenvalue rings from unfolding higher-order exceptional points, *J.*

*Phys. A: Math. Theor.* **41**, 255206 (2008).

- [41] J. Hu, R.-Y. Zhang, Y. Wang, X. Ouyang, Y. Zhu, H. Jia, and C. T. Chan, Non-Hermitian swallowtail catastrophe revealing transitions among diverse topological singularities, *Nat. Phys.* **19**, 1098 (2023).
- [42] H. Zhao, S. Longhi, and L. Feng, Robust light state by quantum phase transition in non-Hermitian optical materials, *Sci. Rep.* **5**, 17022 (2015).
- [43] H. Shen, B. Zhen, and L. Fu, Topological band theory for non-Hermitian Hamiltonians, *Phys. Rev. Lett.* **120**, 146402 (2018).
- [44] S. Yao, F. Song, and Z. Wang, Non-Hermitian Chern bands, *Phys. Rev. Lett.* **121**, 136802 (2018).
- [45] A. Bouhon and R.-J. Slager, Multi-gap topological conversion of euler class via band-node braiding: minimal models, *PT*-linked nodal rings, and chiral heirs, *arXiv preprint arXiv:2203.16741* (2022).
- [46] M. Ezawa, Topological Euler insulators and their electric circuit realization, *Phys. Rev. B* **103**, 205303 (2021).
- [47] W. Zhao, Y.-B. Yang, Y. Jiang, Z. Mao, W. Guo, L. Qiu, G. Wang, L. Yao, L. He, Z. Zhou, *et al.*, Quantum simulation for topological Euler insulators, *Commun. Phys.* **5**, 223 (2022).
- [48] A. Bouhon, T. Bzdušek, and R.-J. Slager, Geometric approach to fragile topology beyond symmetry indicators, *Phys. Rev. B* **102**, 115135 (2020).

## METHODS

### Reference models

The reference models  $H_{\text{Euler}}(\mathbf{k})$ ,  $H_{\text{Chern}}(\mathbf{k})$ , and  $H_{\text{trivial}}(\mathbf{k})$  are described by the  $3 \times 3$  matrices

$$H_{\text{Euler}}(\mathbf{k}) = \begin{pmatrix} g_1(k_x, k_y) & f_1(\mathbf{k}) & f_2(k_x) \\ f_1(\mathbf{k}) & g_1(k_y, k_x) & f_2(k_y) \\ f_2(k_x) & f_2(k_y) & g_2(\mathbf{k}) \end{pmatrix}, \quad (\text{S1})$$

$$H_{\text{Chern}}(\mathbf{k}) = \begin{pmatrix} 0 & h(\mathbf{k}) & \sin k_y \\ -h(\mathbf{k}) & 0 & -\sin k_x \\ -\sin k_y & \sin k_x & 0 \end{pmatrix}, \quad (\text{S2})$$

$$H_{\text{trivial}}(\mathbf{k}) = \begin{pmatrix} 0 & 2 & \sin k_y \\ 2 & 0 & -\sin k_x \\ \sin k_y & -\sin k_x & 0 \end{pmatrix}, \quad (\text{S3})$$

where  $g_1(k_x, k_y) = 1 + \cos k_y - \cos 2k_x$ ,  $g_2(\mathbf{k}) = 2 - \gamma(\cos k_x + \cos k_y) + \cos 2k_x + \cos 2k_y$ ,  $f_1(\mathbf{k}) = \cos(k_x - k_y) - \cos(k_x + k_y)$ ,  $f_2(k) = -\gamma \sin k + \sin 2k$ , and  $h(\mathbf{k}) = 1 - \cos k_x - \cos k_y$ . We set  $\gamma = 0.6$  to maximize the gap between the upper band 3 and the lower two bands 1 and 2 for the Hermitian reference model  $H_{\text{Euler}}(\mathbf{k})$ .

### Proof of the Chern-Euler Duality

#### Auxiliary ‘‘Chern bands’’ from Euler bands

We first show the ‘‘if’’ part of the duality condition: there exists a dual transition satisfying Eq. (1). Starting from a pair of Euler bands  $|\psi_{1,2}(\mathbf{k})\rangle$  of a Hermitian *PT*-symmetric Hamiltonian  $H(\mathbf{k})$ , one may construct a pair of auxiliary ‘‘Chern

bands’’  $|\varphi_{\pm}(\mathbf{k})\rangle = [|\psi_1(\mathbf{k})\rangle \pm i|\psi_2(\mathbf{k})\rangle]/\sqrt{2}$  [20, 39]. We use quotation marks since the complex states  $|\varphi_{\pm}(\mathbf{k})\rangle$  are *not* eigenstates of  $H(\mathbf{k})$ . Such a transformation diagonalizes the non-Abelian Berry curvature matrix  $B(\mathbf{k})$ ,

$$B'_{++}(\mathbf{k}) = -B'_{--}(\mathbf{k}) = iB_{12}(\mathbf{k}). \quad (\text{S4})$$

By comparing Eqs. (3) and (4), it immediately follows that the Chern numbers  $C'_{\pm}$  associated with the bands spanned by  $|\varphi_{\pm}(\mathbf{k})\rangle$  are equal to the Euler number  $\chi$  of the real band pair spanned by  $|\psi_{1,2}(\mathbf{k})\rangle$  in absolute value.

However, at this point the two auxiliary ‘‘Chern bands’’ are mathematical constructions only; they are not eigenstates of  $H(\mathbf{k})$  and are not detectable due to their equal expectation value of energy  $[\text{Re} \langle H(\mathbf{k}) \rangle]$  protected by the *PT* symmetry. To realize them as eigenstates and lift their degeneracy while still preserving a *PT*-symmetric  $H(\mathbf{k})$ , we must introduce non-Hermitian terms to spontaneously break the *PT* symmetry. This can be achieved by first flattening the band pair energy in the Hermitian regime, and then switching on the anti-Hermitian term  $i|\varphi_+(\mathbf{k})\rangle\langle\varphi_+(\mathbf{k})| - i|\varphi_-(\mathbf{k})\rangle\langle\varphi_-(\mathbf{k})|$ . This process does not close the gaps between the band pair and remote bands, hence it is a dual transition.

The above procedure demonstrates that an Euler-band model can be deformed to exhibit Chern bands with  $|C_{\pm}| = |\chi|$ . It also highlights the crucial role of non-Hermiticity in enabling the duality transition. However, in a generic spontaneous *PT*-breaking transition, the initial Euler bands do not split exactly into the two auxiliary Chern bands described above. Spontaneous *PT*-breaking transitions involve ERs sweeping across the BZ, where the eigenvalues coalesce and only a single eigenvector remains [40, 41]. Moreover, away from the ERs, the eigenvectors may deviate significantly from the original pair of real orthonormal eigenvectors  $|\psi_{1,2}(\mathbf{k})\rangle$  of the Hermitian starting point. Correspondingly, the resulting complex bands strongly deviate from the linear combinations  $|\varphi_{\pm}(\mathbf{k})\rangle$  introduced above Eq. (S4). In order to prove the ‘‘only if’’ part of the Chern-Euler duality, we therefore have to resort to some notions from the theory of vector bundles [34] and linear operators [10].

#### Euler number of a real vector bundle

A pair of eigenstates  $|\psi_{1,2}(\mathbf{k})\rangle$  of a Hermitian *PT*-symmetric  $n \times n$  matrix  $H(\mathbf{k})$  spans a two-dimensional subspace  $V(\mathbf{k}) \subset \mathbb{R}^n$ . These subspaces define a real rank-2 vector bundle  $F_{\mathbb{R}}$  over the Brillouin zone (BZ). We consider models  $H(\mathbf{k})$  without weak topology, for which  $F_{\mathbb{R}}$  is an orientable vector bundle, which means that it is possible to consistently choose the orientation of its two basis states  $|\psi_{1,2}(\mathbf{k})\rangle$  across the full BZ. This condition is satisfied for the Hermitian *PT*-symmetric reference models  $H_{\text{Euler}}(\mathbf{k})$  and  $H_{\text{trivial}}(\mathbf{k})$  of the main text. The case of nontrivial weak topology will be discussed at the end of this Section.

The Euler number  $\chi$  is the topological invariant of an *oriented* real rank-2 vector bundle. An oriented vector bundle is an orientable vector bundle equipped with oriented basis.

The Euler number can be calculated as an integral of the off-diagonal element  $B_{12}(\mathbf{k})$  of non-Abelian Berry curvature, see Eq. (3). Reversing the orientation of  $F_{\mathbb{R}}$ , e.g., by exchanging the basis vectors  $|\psi_1(\mathbf{k})\rangle$  and  $|\psi_2(\mathbf{k})\rangle$ , changes the sign of  $B_{12}(\mathbf{k})$  and, hence, of  $\chi$ . Since the choice of the orientation of the vector bundle  $F_{\mathbb{R}}$  associated with the PT-symmetric Hamiltonian  $H(\mathbf{k})$  is arbitrary, the associated Euler number has a sign ambiguity. The sign ambiguity can be resolved by choosing an orientation for the basis vectors  $|\psi_{1,2}(\mathbf{k})\rangle$ .

Although the expression (3) makes explicit reference to the metric on the bundle and two orthonormal basis vectors  $|\psi_{1,2}(\mathbf{k})\rangle$  spanning  $V_{\lambda}(\mathbf{k})$ , the Euler number  $\chi$  is in fact a property of the oriented vector bundle  $F_{\mathbb{R}}$ , independent of the choice of metric and basis [34]. To see its basis-independent, we note that an orientation-preserving transformation of the basis states amounts to the change  $B(\mathbf{k}) \rightarrow O(\mathbf{k})^T B(\mathbf{k}) O(\mathbf{k})$  with  $O(\mathbf{k}) \in SO(2)$ . Since the  $2 \times 2$  matrix  $B(\mathbf{k})$  is anti-symmetric, such a transformation leaves  $B(\mathbf{k})$  and, hence,  $\chi$  invariant.

*Outline of the “only if” part in the proof*

We show that during a generic dual transition we must have  $|C_{\pm}| = |\chi|$ . The key insight behind this Chern-Euler duality relation is that one can always associate an orientable real rank-2 vector bundle  $F_{\mathbb{R}}$  with a pair of bands of a PT-symmetric Hamiltonian  $H(\mathbf{k})$ , irrespective of whether it is an Hermitian or non-Hermitian model with real bands only, a non-Hermitian  $H(\mathbf{k})$  with exceptional rings (ERs), or a model with complex-conjugate energy bands separated by an imaginary spectral gap.

The bundle  $F_{\mathbb{R}}$  is constructed as follows. For non-degenerate real eigenvalues (i.e., away from the ERs), one simply builds the vector spaces  $V(\mathbf{k})$  from the two right-eigenvectors  $|\psi_{1,2}(\mathbf{k})\rangle$  of the band pair, the same way as it is done in the Hermitian case. For complex eigenstates  $|\phi_{+}(\mathbf{k})\rangle = |\phi_{-}(\mathbf{k})\rangle^*$  one uses  $|\psi_1(\mathbf{k})\rangle = \text{Re}|\phi_{+}(\mathbf{k})\rangle$ ,  $|\psi_2(\mathbf{k})\rangle = \text{Im}|\phi_{+}(\mathbf{k})\rangle$  to span  $V(\mathbf{k})$ . (This prescription is independent of the phase of  $|\phi_{+}(\mathbf{k})\rangle$ , as a different phase choice is just a  $GL_2(\mathbb{R})$  transformation within  $V(\mathbf{k})$ .) The only difference with the Hermitian case is that an orthonormalization procedure has to be applied to the basis vectors  $|\psi_1(\mathbf{k})\rangle$  and  $|\psi_2(\mathbf{k})\rangle$  before they can be used to calculate the non-Abelian Berry curvature  $B(\mathbf{k})$  using Eq. (2) [23, 34]. At the ER, the eigenvalues of the band pair coalesce to a single real eigenvalue  $\omega(\mathbf{k})$ . Although the two bands have only a single right-eigenvector, there are two *generalized* right-eigenvectors and one can use them to construct a two-dimensional vector space  $V(\mathbf{k})$  at the ER. (Generalized right-eigenvectors are vectors that are annihilated by  $(\omega(\mathbf{k}) - H(\mathbf{k}))^m$  for large enough  $m$  [10].) Although  $V(\mathbf{k}) \subset \mathbb{R}^n$  is constructed through three distinct procedures for different regimes, we show in the Supplemental Materials Sec. S4 that it varies continuously with  $\mathbf{k}$  across the entire BZ, leading to a globally well-defined real rank-2 vector bundle  $F_{\mathbb{R}}$ .

To prove the Chern-Euler duality, we apply these ideas to a continuous family of PT-symmetric models  $H_{\lambda}(\mathbf{k})$  for which

a band pair goes through a spontaneous PT-breaking transition as a function of the control parameter  $0 \leq \lambda \leq 1$ , without being connected to other bands at any time. The band pair consists of two real bands at  $\lambda = 0$  and of two complex-conjugate bands separated by an imaginary gap for  $\lambda = 1$ . The models  $H_{\lambda}(\mathbf{k})$  of Eq. (5) are an example of such a family. Using the construction outlined in the previous paragraph, an orientable real rank-2 vector bundle  $F_{\mathbb{R},\lambda}$  and its Euler number  $\chi_{\lambda}$  can be associated with the band pair spanning  $V_{\lambda}(\mathbf{k})$  for every  $\lambda$  in the transition. The Euler numbers  $\chi_{\lambda}$  have an over-all sign ambiguity arising from the freedom to choose the orientation of  $F_{\mathbb{R},\lambda}$  for  $\lambda = 0$ . For a fixed orientation, since  $\chi_{\lambda}$  is a topological invariant, it must remain unchanged during the spontaneous PT-breaking transition as long as the two bands stay isolated from other bands at any time (proof in Supplemental Materials S4). In particular, the Euler number  $\chi_{\lambda=1}$  associated with the complex bands at  $\lambda = 1$  must be the same as the Euler number  $\chi = \chi_{\lambda=0}$  associated with the real band pair at the Hermitian starting point at  $\lambda = 0$ .

To complete the proof of  $|C_{\pm}| = |\chi|$  we generalize the procedure preceding Eq. (S4) and show that  $\chi_{\lambda=1}$  is equal to the Chern numbers  $C_{+} = -C_{-}$  of the individual complex bands at  $\lambda = 1$ . At  $\lambda = 1$ , we have complex conjugate eigenstates  $|\phi(\mathbf{k})\rangle = |\psi_1(\mathbf{k})\rangle + i|\psi_2(\mathbf{k})\rangle$  and  $|\phi^*(\mathbf{k})\rangle = |\psi_1(\mathbf{k})\rangle - i|\psi_2(\mathbf{k})\rangle$  across the whole BZ. The real and imaginary parts  $|\psi_1(\mathbf{k})\rangle$  and  $|\psi_2(\mathbf{k})\rangle$  span a two-dimensional real vector bundle  $F_{\mathbb{R},\lambda=1}$  over the BZ. A unitary gauge transformation on  $|\phi(\mathbf{k})\rangle$  — multiplying it with a phase  $e^{i\theta}$  — is equivalent to acting on its real and imaginary parts with a  $SO(2)$  matrix, which shows that the vector bundle spanned by  $|\psi_1(\mathbf{k})\rangle$  and  $|\psi_2(\mathbf{k})\rangle$  is oriented. However,  $|\psi_1(\mathbf{k})\rangle$  and  $|\psi_2(\mathbf{k})\rangle$  are not orthonormal, which prevents direct application of Eq. (S4). To resolve this, we continuously deform the complex eigenstates  $|\phi(\mathbf{k})\rangle \rightarrow |\phi'(\mathbf{k})\rangle \equiv |\psi'_1(\mathbf{k})\rangle + i|\psi'_2(\mathbf{k})\rangle$ , such that the real and imaginary parts  $|\psi'_1(\mathbf{k})\rangle$  and  $|\psi'_2(\mathbf{k})\rangle$  of  $|\phi'(\mathbf{k})\rangle$  are orthonormal. Explicitly,  $|\phi'(\mathbf{k})\rangle$  may be constructed via the Gram-Schmidt orthogonalization procedure,

$$|\phi'(\mathbf{k})\rangle = \frac{|\psi_1(\mathbf{k})\rangle}{\sqrt{n_{11}(\mathbf{k})}} + i \frac{n_{11}(\mathbf{k})|\psi_2(\mathbf{k})\rangle - n_{12}(\mathbf{k})|\psi_1(\mathbf{k})\rangle}{\sqrt{n_{11}(\mathbf{k}) \det n(\mathbf{k})}}, \quad (\text{S5})$$

where

$$n_{\alpha\beta}(\mathbf{k}) = \langle \psi_{\alpha}(\mathbf{k}) | \psi_{\beta}(\mathbf{k}) \rangle, \quad (\text{S6})$$

whereas the continuous deformation  $|\phi(\mathbf{k})\rangle \rightarrow |\phi'(\mathbf{k})\rangle$  may be accomplished by linear interpolation,

$$|\phi_{\mu}(\mathbf{k})\rangle = (1 - \mu)|\phi(\mathbf{k})\rangle + \mu|\phi'(\mathbf{k})\rangle. \quad (\text{S7})$$

The complex vectors  $|\phi_{\mu}(\mathbf{k})\rangle$  have linearly independent real and imaginary parts, ensuring a well-defined Chern number  $C_{\mu}$  as well as an Euler number for all  $0 \leq \mu \leq 1$ . Along the deformation, the two-dimensional spaces spanned by these parts stay the same, hence the Euler number remains  $\chi_{\lambda=1}$ , while the Chern number also remains unchanged since it is a topological invariant:  $C_1 = C_0 \equiv C_{+}$ . For  $\mu = 1$ , real and imaginary parts of  $|\phi_1(\mathbf{k})\rangle = |\phi'(\mathbf{k})\rangle$  are orthonormal, allowing the application of Eq. (S4), which gives  $|C_1| = |\chi_{\lambda=1}|$ .

Therefore, we conclude that  $|C_+| = |C_0| = |\chi_{\lambda=1}| = |\chi|$ , completing the proof. For readers pursuing more rigor, an alternative proof of  $|C_{\pm}| = |\chi_{\lambda=1}|$  without involving the orthonormalization is provided in Supplemental Materials S4.

The dual transition is the physical realization of the ‘‘complexification’’ of an oriented real rank-2 vector bundle: With an oriented real rank-2 vector bundle  $F_{\mathbb{R}}$  spanned by (non necessarily orthonormal) basis vectors  $|\psi_1(\mathbf{k})\rangle$  and  $|\psi_2(\mathbf{k})\rangle$ , one may associate a complex rank-2 bundle  $F_{\mathbb{C}} = \mathbb{C} \otimes F_{\mathbb{R}}$ , spanned by  $|\psi_1(\mathbf{k})\rangle$  and  $|\psi_2(\mathbf{k})\rangle$  with complex coefficients [31]. This complex rank-2 bundle can be decomposed into two complex line bundles,  $F_{\mathbb{C}} = E_{\mathbb{C}} \oplus E_{\mathbb{C}}^*$ , with  $E_{\mathbb{C}}$  spanned by  $|\phi(\mathbf{k})\rangle = |\psi_1(\mathbf{k})\rangle + i|\psi_2(\mathbf{k})\rangle$ . From a topological perspective, the complex bands that appear in PT-symmetric models are precisely those, that can be obtained from such a complexification procedure [31, 34]. All such bands have the property, that the basis vector  $|\phi(\mathbf{k})\rangle$  is linear independent of  $|\phi(\mathbf{k})\rangle^*$  for all  $\mathbf{k}$ , which is ensured by the presence of an imaginary gap in the complex spectrum. For models of size  $n = 2$ , this linear independence condition can be satisfied by topologically trivial complex bundles only. For  $n = 3$ , complex Chern bands in PT-symmetric models exist only if their Chern number is even. Complex Chern bands with Chern number of arbitrary parity exist in PT-symmetric models for  $n \geq 4$ .

#### Weak topology

The Euler topology only exists for PT-symmetric bands without weak topology. A band or a collection of bands in a Hermitian PT-symmetric model  $H(\mathbf{k})$  is said to have weak topology if adiabatic transport of a basis for  $F_{\mathbb{R}}$  around the  $k_x$  or  $k_y$  direction of the BZ-torus reverses its orientation. For such band pairs, no Euler number can be defined due to the non-orientability and they always violate the duality condition. This implies that nontrivial weak topology is an obstruction for opening an imaginary gap in the spontaneous PT-breaking transition: *Only a pair of bands with trivial weak topology can go through a complete spontaneous PT-breaking transition without connecting to other bands.*

## SUPPLEMENTAL MATERIALS

### S1. Berry curvature in non-Hermitian regimes

We clarify cautions of Berry curvature in non-Hermitian regimes. We denote the connection matrix constructed from right eigestates as Hermitian connection matrices. Another common choice of connection is constructed from biorthogonal eigenstates [42–44], which we call the covariant connection. The covariant connection is more difficult to compute or measure as it requires the knowledge of left-eigenstates, too. It has the merit of being  $GL_N(\mathbb{C})$ -covariant (see supplemental material Sec. S6 and Ref. 23), while the Hermitian connection is only  $U(N)$ -covariant. In situations only involving  $U(N)$  gauge structures, the two choices of connection matrices give identical topological results [23, 43], namely

that the invariant polynomials of their curvatures are in the same de Rham cohomology class. One example is Hermitian systems, where all eigenstates are orthonormal and we only meet unitary transformations. The essence of  $GL_N(\mathbb{C})$ -covariance happens when we consider the sum topology of multiple bands that possess EPs or eigenvalue braiding (see supplemental material Sec. S7). In our model, each Chern band is well separated from others by spectral gaps and there is no eigenvalue braiding. The gauge structure of each Chern band can be reduced to  $U(1)$  by normalizing the right eigenstates. This justifies the Hermitian connection in main text. An interesting phenomenon is that the covariant connection matrix exhibits seeming singularities near EPs. A geometric explanation is given in supplemental material Sec. S8.

### S2. Lift of nodal structure protection in spontaneous symmetry breaking regime

The irremovable Dirac points obstruct a real spectral gap (energy gap) within Euler bands [22, 45–47]. We recapitulate this picture and give a general proof based on vector-bundle theory.

Choosing any region  $D$  homeomorphic to a disc in the BZ, a local Euler number  $2\pi i\chi_D = \int_D \bar{B}_{xy}^{12} d^2k - \int_{\partial D} \mathbf{A}^{12} \cdot d\mathbf{k}$  is defined by subtracting the boundary contribution on  $\partial D$ . The nodal points inside  $D$  can be brought together to be annihilated only if  $\chi_D = 0$  [20]. This condition can also be understood as a consequence of winding number compensation. Inside a  $D$ , the two Euler bands are effectively viewed as a two-band system. A PT-symmetric two-band system is protected by a winding number  $W^D$  of  $(d_x, d_z)$ -vectors [19, 20, 32], where  $d_x, d_z$  are the coefficients of the Pauli matrices  $\sigma_x, \sigma_z$ . Every Dirac point carries a nontrivial winding number  $W_j^D$  and  $\chi_D$  is equal to the sum of winding numbers  $\chi_D = \sum_{j \in D} W_j^D / 2 = W_{\partial D} / 2$  [19, 20], where the symbol  $W_{\partial D}$  represents the winding number along  $\partial D$ . If these Dirac points can be annihilated inside  $D$ ,  $W_{\partial D} = 0$ , indicating  $\chi_D = 0$ . Now we have a pair of Euler bands. We partition our BZ into several discs  $D_j$ , the Euler number of the system is the summation of all local Euler numbers:  $\chi = \sum_j \chi_{D_j}$ . If we assume all Dirac points within the Euler bands can be annihilated, we obtain a phase  $\chi_{D_j} = 0$  for all  $j$ . This requires  $\chi = \sum_j \chi_{D_j} = 0$ , resulting in a contradiction.

A more rigorous proof for the forbidden energy gap is done using Whitney sum [34]. If an energy gap is created within the Euler bands without touching other bands, this pair of Euler bands are decomposed into two subbands. This means the Bloch bundle  $F$  of the Euler bands can be written as a sum of two rank-1 Bloch bundles  $F = F_1 \oplus F_2$ . First, assuming  $F_1$  and  $F_2$  are orientable, then their Euler classes are trivial  $e(F_1) = e(F_2) = 0$  (the Euler class of an orientable line bundle must vanish). Using the Whitney sum, the Euler class of  $F$  must also be trivial  $e(F) = e(F_1) \smile e(F_2) = 0$ . This contradicts the nontrivial Euler number of  $F$ , which is the integral of  $e(F)$ . Second, when  $F_1$  and  $F_2$  are not orientable, this is equivalent to saying their first Stiefel-Whitney classes  $w_1(F_j) \in H^1(T^2, \mathbb{Z}_2) = \mathbb{Z}_2 \oplus \mathbb{Z}_2$

are nontrivial, where  $T^2$  is the 2d BZ torus. Let us consider the four-fold covering map of  $T^2$  by itself  $p_{(4)} : T^2 \rightarrow T^2, (k_x, k_y) \rightarrow (2k_x, 2k_y)$ . The pullback bundle  $p_{(4)}^* F_j$  must be orientable, since  $p_{(4)}^* w_1(F_j) = 2w_1(F_j) = 0$ . On the other hand, the pullback bundle  $p_{(4)}^* F$  carries nontrivial Euler class  $e(p_{(4)}^* F) = 4e(F) \neq 0$  in  $H^2(T^2, \mathbb{Z}) = \mathbb{Z}$ . Hence, we are back to the orientable case and still have a contradiction.

In the non-Hermitian regime ERs create the following effects. When non-Hermitian terms are turned on, the Dirac nodes expand into ERs that separate BZ into symmetry-preserving regions and spontaneous symmetry breaking (SSB) regions. In symmetry-preserving regions, we may still define a local winding number of  $(d_x, d_z)$ -vectors [23]. However, there is no winding-number protection in SSB regions [23]. As ERs percolate and span the BZ, all local winding numbers in symmetry-preserving regions are destroyed and we are left with SSB regions (Fig. S1b).

Alternatively, from the vector bundle point of view, an energy gap between the two bands is equal to decomposing the real Bloch bundle into two lower-rank real vector bundles, which is obstructed by the Euler number. In contrast, the imaginary spectral gap (dissipation gap) opening is not a vector bundle decomposition. Instead, it gives a spontaneous complex structure to the real vector bundle (see proof of the Chern-Euler duality). This is a novel effect brought by non-Hermiticity. Thus the dissipation gap is not restricted by the Euler number.

### S3. Homotopy analysis

Homotopy analysis gives a complete view of the topology inside our system. A PT symmetric system is to have a real  $N \times N$  matrix  $H(\mathbf{k})$  with  $\mathbf{k}$  being the control parameters or momenta. We will use the idea of band partition [23] to describe the spectral gaps and topology of the system.

The topology of non-Hermitian PT symmetric systems is captured by the homotopy groups of the matrices having the specified spectral gaps. There are two types of spectral gaps. For those eigenvalues on the real axis, we can sort them from lower energy to higher energy. If the spectrum of the system on the real axis is not connected, there is an energy gap  $\Delta^E$  separating lower-energy eigenvalues and higher-energy eigenvalues. As in the Euler phase, there is a spectral gap between the two lower bands and the higher band. Another type of spectral gap comes from comparing the imaginary parts of the eigenvalues. In PT-symmetric systems, the eigenvalues can detouch from the real axis after spontaneous symmetry breaking. The eigenmodes on the lower complex plane are decaying while the eigenmodes on the upper complex plane are amplifying. Together with those oscillating modes on the real axis, the dynamic properties of the system are determined by the spectral gaps  $\Delta^\tau$  in the imaginary parts of the eigenmodes (Fig. S1a).

From these discussion, we impose the following band/eigenvalue partitions according to the symmetry property of the system. First, we partition our bands/eigenvalues

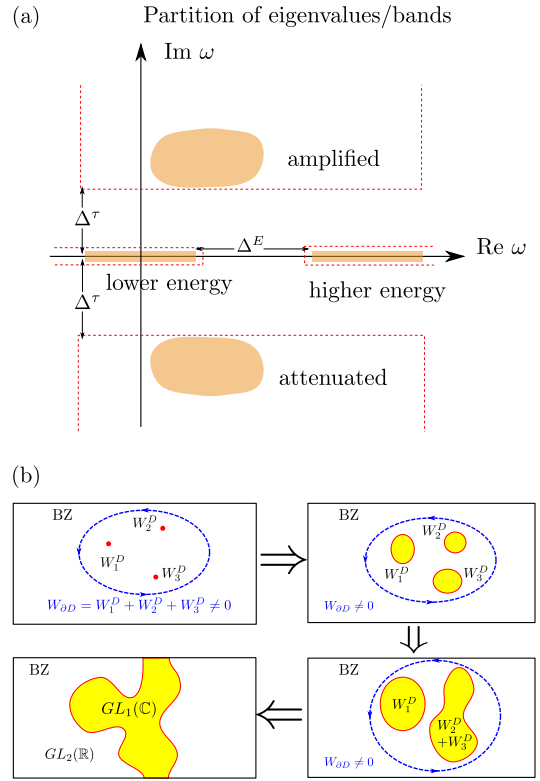


FIG. S1. Partition of eigenvalues/bands and spontaneous symmetry breaking (SSB). (a) When the eigenvalues are on the real axis, we may distinguish them by their real parts, and there can be an energy gap between different connected components in the spectra along the real axis. When the eigenvalues can detach from the real axis, we will also have different connected components on the lower and upper half complex planes. They are distinguished by dissipation gaps. (b) The SSB inside a BZ. Exceptional rings are the boundaries between symmetry-preserving regions and SSB regions. They convert real gauge structures of the eigenstates into complex gauge structures. The protections of the Dirac points are erased after the gauge type shift.

into those on the upper and lower half complex planes, and those on the real axis. On the real axis, if there are more than two bands, we further partition our bands/eigenvalues into higher-energy bands/eigenvalues and lower-energy bands/eigenvalues.

Now we specify to the situations studied in the main text. When all eigenvalues are real, there are two lower-energy bands and one higher energy band. The three eigenvectors  $|\psi_1\rangle, |\psi_2\rangle$  and  $|\psi_3\rangle$  form a  $3 \times 3$  invertible matrix, parametrized by a matrix in  $GL_3(\mathbb{R})$ . Meanwhile, there are gauge transformations within the Hilbert space spanned by the higher-energy eigenvector and the counterpart spanned by the lower-energy eigenvectors. A  $GL_1(\mathbb{R})$  transformation on  $|\psi_3\rangle$  leaves the Hilbert space spanned by  $|\psi_3\rangle$  invariant, while a  $GL_2(\mathbb{R})$  transformation on  $|\psi_1\rangle, |\psi_2\rangle$  leaves  $\text{span}\{|\psi_1\rangle, |\psi_2\rangle\}$  invariant (note that if  $|\psi_1\rangle$  and  $|\psi_2\rangle$  coalesce, we replace them by the sole eigenvector and the generalized eigenvector). Thus for the eigenvector topology, the Hamiltonian gives rise to a map from the PT preserving regions of BZ, denoted as  $BZ_R$ ,

to the real Grassmanian (up to homotopy equivalence):

$$f_1 : \text{BZ}_R \rightarrow \frac{\text{GL}_3(\mathbb{R})}{\text{GL}_2(\mathbb{R}) \times \text{GL}_1(\mathbb{R})}. \quad (\text{S8})$$

When two of the eigenvalues become a complex conjugate pair, the Hamiltonian gives a map from the PT broken regions of BZ, denoted as  $\text{BZ}_C$ , to a generalized mixed Grassmanian [23]:

$$f_2 : \text{BZ}_C \rightarrow \frac{\text{GL}_3(\mathbb{R})}{\text{GL}_1(\mathbb{C}) \times \text{GL}_1(\mathbb{R})}. \quad (\text{S9})$$

This result can be understood as follows: the complex eigenvectors are  $|\psi\rangle, |\psi^*\rangle$ . The real part and the imaginary part of  $|\psi\rangle$  are linearly independent vectors in  $\mathbb{R}^3$ , to ensure that  $|\psi\rangle$  and  $|\psi^*\rangle$  are linearly independent. Together with the third real eigenvector  $|\psi_3\rangle$ , they form a basis of  $\mathbb{R}^3$ , expressed through the column vectors of a real invertible matrix  $\text{GL}_3(\mathbb{R})$ . However, the system allows a gauge transformation:  $|\psi\rangle \rightarrow c|\psi\rangle|\psi^*\rangle \rightarrow c^*|\psi^*\rangle, c \in \mathbb{C} - \{0\}$  and  $|\psi_3\rangle \rightarrow a|\psi_3\rangle, a \in \mathbb{R} - \{0\}$ . These gauge transformations form the group  $\text{GL}_1(\mathbb{C}) \times \text{GL}_1(\mathbb{R})$ . A more rigorous approach taking into account of possible eigenvalue influence is to employ the spectral flattening with oblique projection operators [23]. Note due to the coexistence of two types of gauge structures, the spontaneously symmetry breaking regime (S9) is beyond the symmetric spaces in Cartan's classification. It is not captured by K-theory description or conventional Bott clock.

The lower homotopy groups of the two spaces have been calculated in [23]. We list out the results:

$$\pi_0 \left[ \frac{\text{GL}_3(\mathbb{R})}{\text{GL}_2(\mathbb{R}) \times \text{GL}_1(\mathbb{R})} \right] = 0, \quad (\text{S10})$$

$$\pi_1 \left[ \frac{\text{GL}_3(\mathbb{R})}{\text{GL}_2(\mathbb{R}) \times \text{GL}_1(\mathbb{R})} \right] = \mathbb{Z}_2, \quad (\text{S11})$$

$$\pi_2 \left[ \frac{\text{GL}_3(\mathbb{R})}{\text{GL}_2(\mathbb{R}) \times \text{GL}_1(\mathbb{R})} \right] = 2\mathbb{Z} \cong \mathbb{Z}; \quad (\text{S12})$$

$$\pi_0 \left[ \frac{\text{GL}_3(\mathbb{R})}{\text{GL}_1(\mathbb{C}) \times \text{GL}_1(\mathbb{R})} \right] = 0, \quad (\text{S13})$$

$$\pi_1 \left[ \frac{\text{GL}_3(\mathbb{R})}{\text{GL}_1(\mathbb{C}) \times \text{GL}_1(\mathbb{R})} \right] = 0, \quad (\text{S14})$$

$$\pi_2 \left[ \frac{\text{GL}_3(\mathbb{R})}{\text{GL}_1(\mathbb{C}) \times \text{GL}_1(\mathbb{R})} \right] = 2\mathbb{Z} \cong \mathbb{Z}. \quad (\text{S15})$$

The Euler number in the symmetry-preserving phase comes from Eq. (S12) and the Chern number in the symmetry-breaking phase comes from Eq. (S15).

Note the quotients in the above expressions are effectively ‘‘gauge structures’’ in the eigenstates. This is to say, if we perform these transformations on the eigenstates, the vector space spanned by them is unchanged. In particular, the real and complex general linear groups have the following relation:

$$\text{GL}_2^+(\mathbb{R}) \simeq \text{SO}(2) \cong \text{U}(1) \simeq \text{GL}_1(\mathbb{C}), \quad (\text{S16})$$

where  $\simeq$  means homotopy equivalence and  $\cong$  means diffeomorphism. The expression  $\text{GL}_2^+(\mathbb{R})$  is the real general linear

transformation with a positive determinant. For Euler bands, the gauge structure can indeed be lifted to  $\text{GL}_2^+(\mathbb{R})$  [31, 34] (Euler bands are orientable). In the BZ, ERs are the boundaries separating regions with these two different but homotopy equivalent gauge structures (Fig. S1b).

#### S4. More details of the Chern-Euler duality

##### 1. Continuity of $V(\mathbf{k})$ during the dual transition

Away from an ER, the left-eigenvectors  $|\psi_1(\mathbf{k})\rangle$  and  $|\psi_2(\mathbf{k})\rangle$  associated with a pair of real eigenvalues  $\omega_1(\mathbf{k})$  and  $\omega_2(\mathbf{k})$  are linear independent. The complex left-eigenvectors  $|\phi(\mathbf{k})\rangle$  and  $|\phi(\mathbf{k})\rangle^*$  of a pair of complex conjugate eigenvalues  $\omega(\mathbf{k})$  and  $\omega(\mathbf{k})^*$  are also linear independent, which means that their real and imaginary parts  $|\psi_1(\mathbf{k})\rangle = \text{Re} |\phi(\mathbf{k})\rangle$  and  $|\psi_2(\mathbf{k})\rangle = \text{Im} |\phi(\mathbf{k})\rangle$  are linear independent, too. In both cases,  $|\psi_1(\mathbf{k})\rangle$  and  $|\psi_2(\mathbf{k})\rangle$  span a two-dimensional subspace  $V(\mathbf{k}) \subset \mathbb{R}^n$ . These vector spaces form the vector bundle  $F_{\mathbb{R}}$  away from the ERs. For an EP at  $\mathbf{k} = \mathbf{k}_0$  and eigenvalue  $\omega(\mathbf{k}_0)$  we use the space spanned by the two *generalized right-eigenvectors* to construct the vector space  $V(\mathbf{k}_0)$ .

We now show that the assignment of the two-dimensional vector spaces  $V(\mathbf{k}) \subset \mathbb{R}^n$  to a band pair is continuous in the vicinity of an EP. Hereto, we use that a suitable (non-orthogonal) basis transformation may bring  $H(\mathbf{k}_0)$  to the Jordan canonical form

$$H(\mathbf{k}_0) = \begin{pmatrix} \omega(\mathbf{k}_0) & 1 & 0 & \dots & 0 \\ 0 & \omega(\mathbf{k}_0) & 0 & \dots & 0 \\ 0 & 0 & \omega_3(\mathbf{k}_0) & \dots & 0 \\ \vdots & \vdots & \vdots & \dots & \vdots \\ 0 & 0 & 0 & \dots & \omega_n(\mathbf{k}_0) \end{pmatrix}. \quad (\text{S17})$$

The space  $V(\mathbf{k}_0)$  is spanned by the two generalized eigenvectors at the EP, which are  $|1\rangle \equiv (1, 0, 0, \dots, 0)^T$  and  $|2\rangle \equiv (0, 1, 0, \dots, 0)^T$ . For  $\mathbf{k}$  in the vicinity of the EP, we expand

$$H(\mathbf{k}) = H(\mathbf{k}_0) + dH, \quad (\text{S18})$$

where  $dH = H'_x dk_x + H'_y dk_y$  and  $d\mathbf{k} = \mathbf{k} - \mathbf{k}_0$ . To leading order in  $d\mathbf{k}$ , the eigenvalues and eigenvectors of the band pair are solely determined by the single matrix element  $dH_{21}$ . If  $dH_{21} < 0$ , there are two real eigenvalues  $\omega_{1,2}(\mathbf{k}) = \omega(\mathbf{k}_0) \pm \sqrt{-dH_{21}}$ . If  $dH_{21} > 0$ , there is a pair of complex-conjugate eigenvalues  $\omega(\mathbf{k}_0) \pm i\sqrt{dH_{21}}$ . In both cases, for small  $d\mathbf{k}$  the left-eigenvectors can be calculated explicitly using degenerate perturbation theory taking into  $dH_{21}$  only, followed by non-degenerate perturbation theory to account for the remaining elements of  $dH$ . Since degenerate perturbation theory amounts to a reorganization of the basis vectors, but otherwise keeps  $V(\mathbf{k}_0) = \text{span}(|1\rangle, |2\rangle)$  unchanged, one easily verifies that  $V(\mathbf{k}) \rightarrow V(\mathbf{k}_0)$  if  $d\mathbf{k} \rightarrow 0$ . To leading order in  $d\mathbf{k}$ , the Hamiltonian  $H(\mathbf{k})$  remains a part of the ER if  $dH_{21} = 0$ . Since the generalized eigenspace is a continuous function of  $H(\mathbf{k})$ , in this case, too, one finds that

$V(\mathbf{k}) \rightarrow V(\mathbf{k}_0)$  of  $\delta\mathbf{k} \rightarrow 0$ . Actually, this continuity can be more rigorously defined as a continuous map to the real Grassmannian  $\text{Gr}_2(\mathbb{R}^N)$ , as we shall see in the following section.

## 2. A more rigorous proof using oblique projection operators

We will use the projection operator  $P_{\text{sum}}(\mathbf{k})$  to the two relevant bands to give a more rigorous definition of  $V_\lambda(\mathbf{k})$  and its continuity in  $(\lambda, \mathbf{k})$  during the dual transition. This will also show that  $\chi_\lambda$  is a constant in  $\lambda$ .

The projection operator into the vector space spanned by certain eigenvectors of  $H(\mathbf{k})$  has an elegant compact expression [10, 23]:

$$\sum_{\omega_j \in \mathcal{D}} P_j = \frac{1}{2\pi i} \int_{\partial\mathcal{D}} (z - H)^{-1} dz, \quad (\text{S19})$$

where  $\mathcal{D}$  is a region homeomorphic to a disc on the complex plane of the spectrum. The resolvent  $(z - H)^{-1}$  is the inverse matrix of  $(z - H)$ , which is well defined when  $z$  is not in the spectrum of  $H$ .

We need to consider three cases. In the symmetry-preserving regime, where we have real eigenvectors  $|\psi_1(\mathbf{k}, \lambda)\rangle$  and  $|\psi_2(\mathbf{k}, \lambda)\rangle$ ,  $P_{\text{sum}}(\mathbf{k}, \lambda)$  is the sum of the projection operators  $P_1(\mathbf{k}, \lambda)$  and  $P_2(\mathbf{k}, \lambda)$ . In the spontaneous symmetry-breaking regime, where we have complex pair eigenvectors  $|\phi_+(\mathbf{k}, \lambda)\rangle = |\phi(\mathbf{k}, \lambda)\rangle$  and  $|\phi_-(\mathbf{k}, \lambda)\rangle = |\phi^*(\mathbf{k}, \lambda)\rangle$ ,  $P_{\text{sum}}(\mathbf{k}, \lambda)$  is the sum of the projection operators  $P_+(\mathbf{k}, \lambda)$  and  $P_-(\mathbf{k}, \lambda)$ . When the two eigenvalues are degenerate  $\omega_1(\mathbf{k}, \lambda) = \omega_2(\mathbf{k}, \lambda) = \omega_*$ , for example at EPs,  $P_{\text{sum}}(\mathbf{k}, \lambda)$  is obtained by applying Eq. (S19) for a small disc containing only  $\omega_*$  while excluding other eigenvalues.

We will show that  $P_{\text{sum}}(\mathbf{k}, \lambda)$  is always a real operator, namely, a real  $N \times N$  matrix. And its image when acting on  $\mathbb{R}^N$  is exactly  $V_\lambda(\mathbf{k})$ . The continuity of  $V_\lambda(\mathbf{k})$  results from the continuity of  $P_{\text{sum}}(\mathbf{k}, \lambda)$ . In the cases when the two eigenvalues are non-degenerate, it is straightforward to see the continuity of  $P_{\text{sum}}(\mathbf{k}, \lambda)$ . At their degenerate point, we use Eq. (S19) to show the continuity of  $P_{\text{sum}}(\mathbf{k}, \lambda)$ .

We clarify the notations in the proof. We consider a system of  $N$  bands. Two of them well separated from other  $N - 2$  bands (this means their eigenvalues have no overlap with all other bands) are going through a pairwise spontaneous symmetry breaking (SSB). This SSB is achieved by an interpolation of continuous Hamiltonian  $H(\mathbf{k}, \lambda)$ , where  $\lambda$  is the interpolation parameter. By a re-scaling of  $\lambda$ , we assume  $0 \leq \lambda \leq 1$ . The interpolation Hamiltonian is now a map from  $\text{BZ} \times [0, 1]$  to  $N \times N$  real matrices. For simplicity, we use  $\widetilde{\text{BZ}}$  to represent  $\text{BZ} \times [0, 1]$ . The sum projection into these two relevant bands in **main result** is written as  $P_{\text{sum}}(\mathbf{k}, \lambda)$ . Before the SSB, we denote the two relevant eigenvalues as  $\omega_1(\mathbf{k}, \lambda)$  and  $\omega_2(\mathbf{k}, \lambda)$  (with corresponding eigenvectors  $|\psi_1\rangle$  and  $|\psi_2\rangle$ ). After the SSB, the eigenvalues are denoted as  $\omega(\mathbf{k}, \lambda), \omega^*(\mathbf{k}, \lambda)$  with their corresponding eigenvectors  $|\phi_+\rangle = |\phi\rangle, |\phi_-\rangle = |\phi^*\rangle$ . Their real and imaginary parts are  $|\phi_\pm\rangle = |\psi_R\rangle \pm i|\psi_I\rangle$ .

We assume there is no remote band touching during the transition:  $\omega_i(\mathbf{k}, \lambda) \neq \omega_j(\mathbf{k}, \lambda)$  for all  $i = 1, 2, \pm$ , all  $j \neq 1, 2, \pm$  and all  $\mathbf{k}, \lambda$ . Note here we only exclude local band touchings (level crossings at the same  $\mathbf{k}, \lambda$ ). This is a more general situation where trivial spectral overlaps between bands at different  $\mathbf{k}, \lambda$  are allowed.

*Images of  $P_{\text{sum}}(\mathbf{k})$ :* We first verify the relation between the sum projection operator and the real vector bundle structure of rank 2 in regions of  $\widetilde{\text{BZ}}$  without degeneracy between the two relevant bands. We call these regions non-degenerate regions of the  $\widetilde{\text{BZ}}$ . In non-degenerate regions, the two eigenvectors are distinct and we can express everything in terms of them. We denote the regions of  $\widetilde{\text{BZ}}$  where the two relevant eigenvalues are real as  $\widetilde{\text{BZ}}_R$ . The regions of  $\widetilde{\text{BZ}}$  where the two relevant eigenvalues are complex as  $\widetilde{\text{BZ}}_C$ . In  $\widetilde{\text{BZ}}_R$ , we have two real eigenvectors  $|\psi_1(\mathbf{k}, \lambda)\rangle$  and  $|\psi_2(\mathbf{k}, \lambda)\rangle$ . The sum projection into the space  $V_\lambda(\mathbb{R})$  spanned by  $|\psi_1(\mathbf{k}, \lambda)\rangle$  and  $|\psi_2(\mathbf{k}, \lambda)\rangle$  is simply given by  $P_{\text{sum}}(\mathbf{k}, \lambda) = P_1(\mathbf{k}, \lambda) + P_2(\mathbf{k}, \lambda)$ , where  $P_j(\mathbf{k}, \lambda) = |\psi_j(\mathbf{k}, \lambda)\rangle\langle\psi_j(\mathbf{k}, \lambda)|$  and  $\langle\tilde{\psi}_j|$  are the corresponding biorthogonal left eigenvectors. Note although this is not an orthogonal projection in the presence of non-Hermiticity,  $\ker P_{\text{sum}} \not\perp \text{img } P_{\text{sum}}$ , the operator  $P_{\text{sum}}$  still gives us a map from  $\widetilde{\text{BZ}}_R$  to the space of two dimensional subspaces of  $\mathbb{R}^N$ , the Grassmannian  $\text{Gr}_2(\mathbb{R}^N)$ , via:

$$\widetilde{\text{BZ}}_R \rightarrow \text{Gr}_2(\mathbb{R}^N) : (\mathbf{k}, \lambda) \mapsto \text{img } P_{\text{sum}}(\mathbf{k}, \lambda). \quad (\text{S20})$$

This is a continuous map on  $\widetilde{\text{BZ}}_R$ , as the eigenvectors are continuous away from the EP [10].

On  $\widetilde{\text{BZ}}_C$ , the relation between the total projection and the rank-2 real vector bundle structure is not so obvious. Let us see how it unfolds for these complex eigenvectors. On  $\widetilde{\text{BZ}}_C$ , the two eigenvalues correspond to the following block in the canonical form of  $H(\mathbf{k}, \lambda)$ :

$$\left( |\phi\rangle, |\phi^*\rangle \right) \begin{pmatrix} \omega & 0 \\ 0 & \omega^* \end{pmatrix} \begin{pmatrix} \langle\tilde{\phi}| \\ \langle\tilde{\phi}^*| \end{pmatrix}, \quad (\text{S21})$$

where  $|\phi\rangle = |\phi_+\rangle$  corresponds to the eigenvalue on the lower half complex plane and  $|\phi^*\rangle = |\phi_-\rangle$  corresponds to the upper half complex plane partner. The two eigenvectors are biorthogonal:  $\langle\tilde{\phi}| \cdot |\phi^*\rangle = \langle\tilde{\phi}^*| \cdot |\phi\rangle = 0$  and  $\langle\tilde{\phi}| \cdot |\phi\rangle = \langle\tilde{\phi}^*| \cdot |\phi^*\rangle = 1$ . Now the eigenvectors are complex. We decompose them into their real and imaginary parts:  $|\phi\rangle = |\psi_R\rangle + i|\psi_I\rangle$ ,  $\langle\tilde{\phi}| = \langle\tilde{\psi}_R| + i\langle\tilde{\psi}_I|$ . There exist a series of relations between these vectors. First of all, the vectors  $|\psi_R\rangle$  and  $|\psi_I\rangle$  are linearly independent, and so are  $\langle\tilde{\psi}_R|$  and  $\langle\tilde{\psi}_I|$ . Secondly, due to the biorthogonal relations, we can verify these real vectors are also biorthogonal:  $\langle\tilde{\psi}_\alpha| \psi_\beta\rangle = \delta_{\alpha\beta}/2$ . The sum projection for this pair of complex eigenvalues is

$$\begin{aligned} P_{\text{sum}}(\mathbf{k}, \lambda) &= |\phi(\mathbf{k}, \lambda)\rangle\langle\tilde{\phi}(\mathbf{k}, \lambda)| + |\phi(\mathbf{k}, \lambda)^*\rangle\langle\tilde{\phi}(\mathbf{k}, \lambda)^*| \\ &= 2 \left[ |\psi_R(\mathbf{k}, \lambda)\rangle\langle\tilde{\psi}_R(\mathbf{k}, \lambda)| + |\psi_I(\mathbf{k}, \lambda)\rangle \right. \\ &\quad \left. \times \langle\tilde{\psi}_I(\mathbf{k}, \lambda)| \right], \quad \text{for } (\mathbf{k}, \lambda) \in \widetilde{\text{BZ}}_C. \quad (\text{S22}) \end{aligned}$$

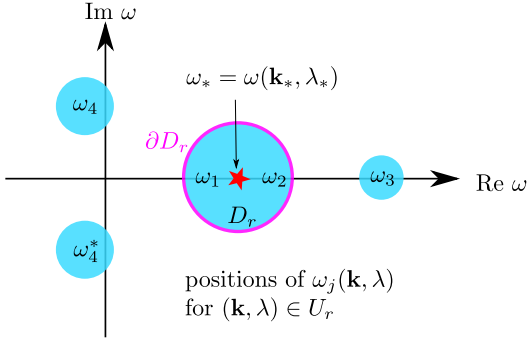


FIG. S2. How to choose the enclosing disc  $D$  on the complex plane of spectrum. The blue discs represent the approximate region of all eigenvalues  $\omega_j$  for  $\mathbf{k}, \lambda$  in a neighbourhood of the EP.

This is exactly a projection operator into the real 2-dimensional subspace of  $\mathbb{R}^N$  spanned by  $|\psi_R\rangle$  and  $|\psi_I\rangle$ . According to this relation, in the situation of a pair of complex eigenvalues, the sum projection still defines a map from  $\widetilde{\text{BZ}}_C$  to the space of two dimensional subspaces of  $\mathbb{R}^N$ :

$$\widetilde{\text{BZ}}_C \rightarrow \text{Gr}_2(\mathbb{R}^N) : (\mathbf{k}, \lambda) \mapsto \text{img } P_{\text{sum}}(\mathbf{k}, \lambda). \quad (\text{S23})$$

Again the above map is continuous on  $\widetilde{\text{BZ}}_C$ . Albeit the two eigenvectors are complex, their sum projection is projecting every real vector in  $\mathbb{R}^N$  into the subspace spanned by the real and the imaginary parts of the eigenvector, i.e.,  $V_\lambda(\mathbf{k})$ . Notice that it does not matter which eigenvector is chosen to take the real and the imaginary parts, since the corresponding components of  $|\phi\rangle$  and  $|\phi\rangle^*$  span the same real 2-dimensional subspace. They only differ by choices of orientations in  $\text{img } P_{\text{sum}}$ .

Combining the two cases, the sum projection operator always gives a continuous map from non-degenerate regions of  $\widetilde{\text{BZ}}$  to the Grassmannian  $\text{Gr}_2(\mathbb{R}^N)$ , leading to a continuous  $V_\lambda(\mathbf{k})$  for these regions. In the next step, we will show that the sum projection is also continuous on degenerate regions of  $\widetilde{\text{BZ}}$ . Therefore the map to  $\text{Gr}_2(\mathbb{R}^N)$  is continuous throughout the whole phase transition process.

*Continuity at EPs:* We now look at the continuity of the map within the degenerate regions of  $\widetilde{\text{BZ}}$ . We first prove  $(\mathbf{k}, \lambda) \mapsto P_{\text{sum}}(\mathbf{k}, \lambda)$  is also continuous over every degenerate point. Then using the continuity of the map  $P_{\text{sum}}(\mathbf{k}, \lambda) \mapsto \text{img } P_{\text{sum}}(\mathbf{k}, \lambda)$  of constant-rank projection operators, we prove that the map from  $\widetilde{\text{BZ}}$  to  $\text{Gr}_2(\mathbb{R}^N)$  is continuous everywhere. This procedure can be represented as the following composition map:

$$\widetilde{\text{BZ}} \rightarrow \text{Gr}_2(\mathbb{R}^N) : (\mathbf{k}, \lambda) \mapsto P_{\text{sum}} \mapsto \text{img } P_{\text{sum}}. \quad (\text{S24})$$

A degeneracy between the two relevant bands takes place if and only if the two eigenvalues are approaching each other and eventually become equal. At the degenerate point, it is not convenient to use the language of eigenvectors, as they become singular. However, the sum projection is still well defined, via the integral expression Eq. (S19). We denote the degenerate point as  $(\mathbf{k}_*, \lambda_*)$  and the corresponding eigenvalue

at this point as  $\omega_* \in \mathbb{R}$ . Around  $(\mathbf{k}_*, \lambda_*)$ , we always denote the two eigenvalues as  $\omega_1(\mathbf{k}, \lambda)$  and  $\omega_2(\mathbf{k}, \lambda)$ , regardless of whether they are real or a conjugate pair, or even equal. Since the eigenvalues are always continuous in  $H$  [10], for any (open) disc region  $D_r$  of radius  $r$  centered at  $\omega_*$ , there is a neighbourhood  $U_r$  of  $(\mathbf{k}_*, \lambda_*)$  such that for all  $(\mathbf{k}, \lambda) \in U_r$ ,  $\omega_1(\mathbf{k}, \lambda), \omega_2(\mathbf{k}, \lambda) \in D_r$ . As the two bands do not touch any other remote bands during the interpolation, we can let  $U_r$  and  $D_r$  small enough such that all other eigenvalues of  $H(\mathbf{k}, \lambda)$  are outside  $\overline{D}_r$  for all  $(\mathbf{k}, \lambda) \in U_r$ . With these definitions, we can safely evaluate  $P_{\text{sum}}(\mathbf{k}, \lambda)$  by choosing  $D = D_r$ :

$$P_{\text{sum}}(\mathbf{k}, \lambda) = \frac{1}{2\pi i} \int_{\partial D_r} [z - H(\mathbf{k}, \lambda)]^{-1} dz, \quad \forall (\mathbf{k}, \lambda) \in U_r. \quad (\text{S25})$$

We prove that Eq. (S25) is a continuous map at  $(\mathbf{k}_*, \lambda_*)$ . This step is similar to the proof of continuity for non-Hermitian spectral flattening (Ref. 23 Appendix. G). Denote  $A = z - H(\mathbf{k}_*, \lambda_*)$  and  $B = z - H(\mathbf{k}_2, \lambda_2)$  with  $(\mathbf{k}_2, \lambda_2) \in U_r$ . By choosing  $(\mathbf{k}_2, \lambda_2)$  close enough to  $(\mathbf{k}_*, \lambda_*)$ , we can let  $\delta = \|A - B\|$  arbitrarily small. Then the difference between their reverse is

$$\begin{aligned} \|A^{-1} - B^{-1}\| &= \|B^{-1}(B - A)A^{-1}\| \\ &\leq \|B^{-1}\| \cdot \|(B - A)\| \cdot \|A^{-1}\| \\ &= \|B^{-1}\| \cdot \|A^{-1}\| \delta. \end{aligned} \quad (\text{S26})$$

As  $A$  invertible for  $z \in \partial D_r$ ,  $\|A^{-1}\|$  is a continuous bounded function in  $z$ . The value of  $\|B^{-1}\|$  is estimated as below:

$$\begin{aligned} \|B^{-1}\| &= \|A^{-1} + B^{-1}(A - B)A^{-1}\| \\ &\leq \|A^{-1}\| + \|B^{-1}\| \cdot \|A^{-1}\| \delta, \end{aligned} \quad (\text{S27})$$

$$\rightarrow \|B^{-1}\| \leq \frac{\|A^{-1}\|}{1 - \|A^{-1}\| \delta}. \quad (\text{S28})$$

Combining Eq. (S26) and Eq. (S28), we obtain the bounding equation for the difference between resolvent:

$$\|A^{-1} - B^{-1}\| \leq \frac{\|A^{-1}\|^2 \delta}{1 - \|A^{-1}\| \delta}. \quad (\text{S29})$$

The right-hand-side goes to zero as  $\delta \rightarrow 0$ . To estimate the integral Eq. (S25), we notice that  $\|A^{-1}\|/(1 - \|A^{-1}\| \delta)$  is a continuous function on  $\partial D_r$ , as long as  $\delta$  is chosen to be small enough. We may denote its supremum as  $w$ . Then the difference between the total projections is bounded by

$$\|P_{\text{sum}}(\mathbf{k}_2, \lambda_2) - P_{\text{sum}}(\mathbf{k}_*, \lambda_*)\| \leq w r \delta, \quad (\text{S30})$$

for all  $(\mathbf{k}_2, \lambda_2)$  close enough to  $(\mathbf{k}_*, \lambda_*)$ . So this proves the continuity of the projection  $P_{\text{sum}}(\mathbf{k}, \lambda)$  at the degenerate points of the two relevant bands. Together with what we have already shown,  $P_{\text{sum}}(\mathbf{k}, \lambda)$  is continuous over the whole region  $\widetilde{\text{BZ}} = \text{BZ} \times [0, 1]$ .

The last thing we need to verify in Eq. (S24) is that  $\text{img } P_{\text{sum}}$  is continuous in  $P_{\text{sum}}$ . It suffice to check the continuity at a neighbourhood for arbitrary projection operator  $P$ . First, note that a continuous  $P(\mathbf{k}, \lambda)$  has a fixed rank

( $\text{rank } P = \text{tr } P$ ). Consider the space  $O^{(2)}$ , the space of rank-2 projection operators in  $\mathbb{R}^N$ , and taking an arbitrary point  $P \in O^{(2)}$ . We build a map from  $U$ , a neighbourhood of  $P$  in  $O^{(2)}$ , to  $V_2(\mathbb{R}^N)$ , the Stiefel manifold [34]. We can pick two fixed vectors  $v_1, v_2 \in \mathbb{R}^N$  such that  $Pv_1$  and  $Pv_2$  are linearly independent. Then there is a neighbourhood  $U$  of  $P$  such that  $P'v_1$  and  $P'v_2$  are independent for all  $P' \in U$ . This defines a continuous map from  $U$  to  $V_2(\mathbb{R}^N)$  on  $U$ . Using the canonical map  $V_2(\mathbb{R}^N) \rightarrow \text{Gr}_2(\mathbb{R}^N)$ , the map  $P_{\text{sum}} \mapsto \text{img } P_{\text{sum}}$  is continuous on  $U$ . This completes the proof of continuity of  $\widetilde{\text{BZ}} \rightarrow \text{Gr}_2(\mathbb{R}^N)$ .

Recall  $\widetilde{\text{BZ}} = \text{BZ} \times [0, 1]$ . At each  $\lambda \in [0, 1]$ , we have a real vector bundle  $F_{\mathbb{R}, \lambda}$  over  $\text{BZ}$  with Euler number denoted by  $\chi_\lambda$ . The map  $\widetilde{\text{BZ}} \rightarrow \text{Gr}_2(\mathbb{R}^N)$  is an homotopy between  $\text{BZ} \times \{0\} \rightarrow \text{Gr}_2(\mathbb{R}^N)$  and  $\text{BZ} \times \{1\} \rightarrow \text{Gr}_2(\mathbb{R}^N)$ , which induces an isomorphism between two vector bundles at  $\lambda = 0$  and  $\lambda = 1$ . Therefore, we have  $\chi_{\lambda=0} = \chi_{\lambda=1}$ : the Euler number of the real vector bundle  $F^{RI}$  spanned by  $|\psi_R(\mathbf{k})\rangle, |\psi_I(\mathbf{k})\rangle$  is equal to that of the initial symmetry-preserving bands.

### 3. Proof for $|\chi_{\lambda=1}| = |C_\pm|$

To prove  $|\chi_{\lambda=1}| = |C_\pm|$ , independent of the shape of the  $\text{BZ}$ , we employ the fact [31, 34] that the Chern class of a complex line bundle is equal to the Euler class of its underlying rank-2 real vector bundle. The eigenstate  $|\phi(\mathbf{k})\rangle$  spans a complex line bundle  $E_C$ . At each  $\mathbf{k}$ , this bundle gives an one dimensional complex vector space  $\widetilde{V}(\mathbf{k})$ . An one dimensional complex vector space can always be regarded as a two-dimensional real vector space  $\widetilde{V}_R(\mathbf{k})$ , called its realification [31]. This  $\widetilde{V}_R(\mathbf{k})$  gives an underlying rank-two real vector bundle  $E_R$  corresponding to  $E_C$ , for which we have  $\chi(E_R) = C(E_C) = C_\pm$ .

We show that the underlying real vector bundle  $E_R$  corresponding to  $|\phi(\mathbf{k})\rangle$  is isomorphic to the bundle  $F_{\mathbb{R}, 1}$  spanned by  $|\psi_R(\mathbf{k})\rangle, |\psi_I(\mathbf{k})\rangle$ . So  $\chi(E_R) = \pm\chi_{\lambda=1}$  with the sign depending on the choice of orientation for the isomorphism. This completes the proof. The isomorphism can be built as follows. For each  $\mathbf{k}$ , we pick  $|\phi_+(\mathbf{k})\rangle$  and expand it as  $|\psi_R(\mathbf{k})\rangle + i|\psi_I(\mathbf{k})\rangle$ . Then a general complex vector  $(a + ib)|\phi_+(\mathbf{k})\rangle \in \widetilde{V}(\mathbf{k})$ ,  $a, b \in \mathbb{R}$  is first mapped to a vector  $(a, b) \in \widetilde{V}_R(\mathbf{k})$ , then mapped to  $a|\psi_R(\mathbf{k})\rangle - b|\psi_I(\mathbf{k})\rangle$  in  $\text{span}\{|\psi_R(\mathbf{k})\rangle, |\psi_I(\mathbf{k})\rangle\} = V_1(\mathbf{k})$ . We can verify that this map is  $\mathbb{R}$ -linear, invertible, and does not depend on the phase chosen for  $|\phi_+(\mathbf{k})\rangle$  (in fact, this map is simply  $c|\phi_+(\mathbf{k})\rangle \mapsto \text{Re } c|\psi_+(\mathbf{k})\rangle$ , where  $\text{Re}$  is globally well-defined). So this is indeed a vector bundle isomorphism.

Note that in the proof of this section, we do not need any topological property of the  $\text{BZ}$  torus apart from compactness. Therefore the Chern-Euler duality applies to Euler bands and Chern bands on any two-dimensional compact surfaces.

## S5. Wilson loop results for the dual transition

We show how to use Wilson loop to find out the topological invariants and interpret the dual transition.

First, we construct the Wilson loop operator from successive action of projection operators. We take the loop in the direction of  $k_y$  along fixed  $k_x$ . The start and end point is chosen to be  $(k_x, -\pi) = (k_x, \pi)$ . The operator is given by

$$O_w(k_x) = \lim_{\delta \rightarrow 0} \prod_n P(k_x, \pi) P(k_x, \pi - \delta) \dots P(k_x, \pi - n\delta) \dots P(k_x, -\pi). \quad (\text{S31})$$

The projection operator can be obtained from the  $H$  directly. As we have seen in Eq. (S19), the projection operator in the non-Hermitian regime still only relies on the Hamiltonian matrix and is  $\text{GL}_n(\mathbb{R}/\mathbb{C})$ -gauge-independent. To obtain it, we do a Jordan decomposition  $H = V^{-1}D_JV$ . The matrix  $D_J$  is a block-diagonal matrix with Jordan blocks corresponding to eigenvalues of  $H$ . To find out the projection operator  $P_j$  for the  $j$ -th eigenvalue  $\omega_j$  (it may be  $n$ -fold degenerate), we replace the  $n \times n$  (Jordan) block corresponding to  $\omega_j$  in  $D_J$  by an  $n$ -dimensional identity matrix, and set all other elements of  $D_J$  to zero. Via this, we obtain an  $N \times N$  matrix  $e_j$ . Then  $P_j$  is given by  $P_j = V^{-1}e_jV$ . This method has the merit of gauge independence and one can verify this is indeed a well-defined projection  $P_j^2 = P_j$ .

For the Hermitian Euler bands, we take the projection operator to be the total projection on the Euler bands  $P(\mathbf{k}) = P_{\text{sum}}(\mathbf{k}) = |\psi_1(\mathbf{k})\rangle\langle\psi_1(\mathbf{k})| + |\psi_2(\mathbf{k})\rangle\langle\psi_2(\mathbf{k})|$ , numerically obtained via the methods in the last paragraph. The loop operator sandwiched between the eigenstates defines a linear transformation matrix:

$$W_{ij}(k_x) = \langle\psi_i(k_x, -\pi)|O_w(k_x)|\psi_j(k_x, -\pi)\rangle, i, j \in \{1, 2\}. \quad (\text{S32})$$

This matrix can be uniquely polar decomposed into the product of an orthogonal matrix  $U$  and a positive definite symmetric matrix  $S$  (in practice, we can do singular value decomposition  $W = V_1\Sigma V_2^{-1}$  and set the diagonal matrix to identity to obtain  $U = V_1V_2^{-1}$ ):

$$W_{ij}(k_x) = \sum_l U_{il}(k_x)S_{lj}(k_x). \quad (\text{S33})$$

The eigenvalues of the  $2 \times 2$  orthogonal matrix  $U_{ij}(k_x)$  are a pair of complex conjugate numbers  $\{\exp[i\theta(k_x)], \exp[-i\theta(k_x)]\}$ . As a periodic function of  $k_x$ , the phase  $\theta(k_x)$  increases by an integer multiple of  $2\pi$  when  $k_x$  goes from  $-\pi$  to  $\pi$ . This integer is the Euler number  $\chi$  [48]. The result for our 3-band model  $H_{\text{Eu}}(\mathbf{k})$  is shown in Fig. S3a.

In Sec. S4, we showed that the oblique projection  $P_{\text{sum}}$  is continuous even in the regime with exceptional rings. With this property, it is possible to study the corresponding Wilson loop of  $P_{\text{sum}}$  for  $H_{0 < \lambda < 1}$ . The operator  $P_{\text{sum}}$  are constructed by Jordan-decomposing  $H_\lambda$ , replacing the block related to the pairs of bands by identity matrix and all other elements by 0. The operator  $O_w$  is constructed as Eq. (S31). The

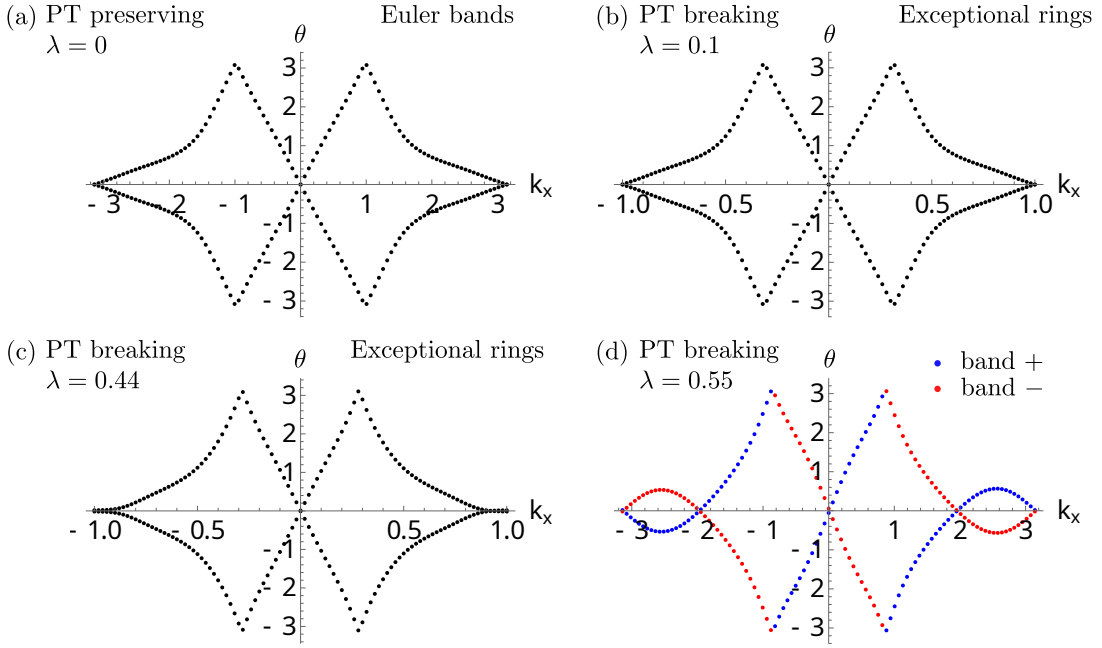


FIG. S3. Wilson loop phases during the spontaneous Chern-Euler transition. (a) The Euler bands in the symmetry-preserving regime. The Wilson loop operator has two complex conjugate eigenvalues. Their phases are going through  $\pm 2\chi\pi$  winding. (b)-(c) The Wilson loops correspond to the summation projection operator of the two bands going through the SSB. Even exceptional rings appear, the projection operator is continuous and deforms adiabatically from the initial Euler bands. (d) The Chern bands in the SSB regime. Each Chern band possesses its own Wilson loop operator, whose action is a complex number inside the band. The phase of this complex number does a  $2C\pi$  rotation.

only difference from Hermitian regime is that the matrix element (S32) is slightly harder, since we may touch exceptional rings. The strategy is to first find out the two eigenvectors of  $P_{\text{sum}}(k_x, -\pi)$  corresponding to the unit eigenvalue. Then we orthonormalise these two eigenvectors into  $v_1(k_x)$  and  $v_2(k_x)$ . The  $2 \times 2$  matrix  $W_{ij}(k_x)$  is now obtained by replacing  $|\psi_{1,2}(k_x, -\pi)\rangle$  by  $v_{1,2}(k_x)$  in Eq. S32:

$$W_{ij}(k_x) = \langle v_i(k_x) | O_w(k_x) | v_j(k_x) \rangle, i, j \in \{1, 2\}. \quad (\text{S34})$$

Doing a similar polar decomposition as Eq. S33, we extract the eigenphases of the orthogonal component. Their phase winding are plotted in Fig. S3b-c. We can see the topology is preserved through the spontaneous symmetry breaking process, in spite of the presence of exceptional rings.

The Wilson loop approach is also applicable for Chern bands. For a Chern band  $|\psi_j(\mathbf{k})\rangle$ , we take the projection operator in Eq. (S31) to be  $P(\mathbf{k}) = P_j(\mathbf{k}) = |\psi_j(\mathbf{k})\rangle\langle\psi_j(\mathbf{k})|$ . This matrix is numerically obtained by Jordan decomposition  $H = V^{-1}D_JV$  and replacing the Jordan block in  $D_J$  corresponding to the band  $j$  by 1 and all other elements by 0. The transformation matrix  $W$  is now a complex number  $c \neq 0$ . The polar decomposition simply gives the phase of  $c$ , whose winding when  $k_x$  is swept from  $-\pi$  to  $\pi$  gives the Chern number. We give this results for  $H_{\lambda=0.55}$  in Fig. S3d. Since now the two bands  $+, -$  are separated by a dissipation gap, each of their projections  $P_{\pm}$  gives a Wilson loop phase winding  $\pm 4\pi$ . Putting them together, we obtain a pattern joint pattern which shares the same topology as the original Euler phase but with geometric distinctions.

By comparing results in Fig. S3, we see when the symmetry is completely broken and an imaginary eigenvalue gap is opened, the original Euler topology is inherited by each individual Chern bands. There are some geometric differences between the Wilson loops corresponding to  $P_{\text{sum}}$  and  $P_+, P_-$ , due to basis choices. Nevertheless, they do not alter the topological information.

## S6. Covariant connection VS Hermitian “connection”

We clarify the issues with Berry connection and curvature in this section. We start from basic introduction to vector bundles and the connection on it. In this section, we use the term “gauge transformation” to refer to basis transformation inside a vector bundle, as in many physical literature.

We have a wave function  $|\psi_j(\mathbf{k})\rangle$  depending on parameters  $\mathbf{k} = (k_1, k_2, \dots)$ . The wave functions different by a scalar factor represent the same physical state. In this sense, each physical state corresponds to an one-dimensional vector space and several distinct states  $|\psi_1(\mathbf{k})\rangle, |\psi_2(\mathbf{k})\rangle, \dots$  can form a higher dimensional vector space at  $\mathbf{k}$ . The parameters  $\mathbf{k}$  define a base space where the vector spaces grow upon. A natural language to describe such structure is vector bundle, if the vector spaces are continuous with respect to  $\mathbf{k}$ . The dimension of the vector space is called the rank of the vector bundle. A common physical situation is the wave functions coming out of the eigenstates of a Hamiltonian matrix  $H(\mathbf{k})$ . The vector space spanned by each eigenstate is usually contin-

uous in  $\mathbf{k}$  when there is no level crossings, or nontrivial loops in the base space. In this situation, each band corresponds to a rank-1 vector bundle, or a line bundle. When a singularity or discontinuity of a single-level wave function takes place, we may look at the combined vector space including all levels associated with the singularity. Usually the combined vector space is continuous and permits a vector bundle description. This has also been seen in our proof of the Chern-Euler duality.

The singularities of level crossings necessitate gauge transformations. For example, in 2D systems, the eigenstate wave functions are not continuous at the Dirac node between two bands, so is the individual vector space spanned by each eigenstate. However, we can always perform a  $SO(2)$  gauge transformation on the two eigenstates to explicitly see the sum vector space spanned by them is continuous at the Dirac point [20]. Due to this continuity, it is possible to describe the two eigenstates near the Dirac node using the language of rank-2 vector bundles.

Once we have a well-defined vector bundle, geometric quantities naturally appear. A geometric connection tells us how to take directional derivatives for vector fields on a vector bundle, in other words, how to compare the vector spaces at different points of the base space. As an intrinsic property of the vector bundle, the connection should not rely on which basis is chosen. Therefore the geometric connection is covariant under a gauge transformation on the eigenstates,.

In Hermitian systems, we usually only need to perform orthogonal or unitary gauge transformations, as the example around Dirac points. In non-Hermitian systems, this may not be enough. An important example is the EP, where the eigenstates overlap and a unitary gauge transformation cannot restore the correct smooth basis. Another example is the braiding of eigenvalues. There the eigenstates swap. Since the eigenstates are not orthogonal to each other, there may be no guarantee that the swap matrix of the eigenstates is unitary or orthogonal. Instead, we have to replace the usual orthogonal/unitary transformations by general linear transformations  $GL_N(\mathbb{R}), GL_N(\mathbb{C})$ .

Motivated by the above requirements, a *covariant connection* is defined by [23]:

$$\nabla_a |\psi_j(\mathbf{k})\rangle \equiv \partial_a |\psi_j(\mathbf{k})\rangle = -i \sum_{j'} \mathcal{A}_a^{j'j}(\mathbf{k}) |\psi_{j'}(\mathbf{k})\rangle, \quad (\text{S35})$$

where  $|\psi_j\rangle$  is the right eigenvector of the  $j$ -th band. We denote the corresponding biorthogonal left eigenvector as  $\langle \tilde{\psi}_j |$ . The first equation is the definition of the geometric connection  $\nabla$ , while the second equation is to expand  $\partial_a |\psi_j(\mathbf{k})\rangle$  in terms of the eigenbasis. The coefficients form the connection matrix  $\mathcal{A}_a^{j'j}$ . For diagonalizable matrices, we can use the biorthogonal relation  $\langle \tilde{\psi}_i(\mathbf{k}) | \psi_j(\mathbf{k}) \rangle = \delta_{ij}$  [for non-diagonalizable matrices, we need to include generalised eigenvectors. A better way is to use the basis-independent expression Eq. (S46)]. The connection matrix is

$$\mathcal{A}_a^{ij}(\mathbf{k}) = i \langle \tilde{\psi}_i(\mathbf{k}) | \partial_a \psi_j(\mathbf{k}) \rangle. \quad (\text{S36})$$

The covariance under gauge transformation is computed directly from Eq. (S35). If we choose another basis  $|\psi'_j(\mathbf{k})\rangle =$

$\sum_i |\psi_i(\mathbf{k})\rangle V_{ij}(\mathbf{k})$  on  $F$  [the biorthogonal left eigenvectors transform as  $\langle \tilde{\psi}_j(\mathbf{k}) | \rightarrow \sum_i \langle \tilde{\psi}_i(\mathbf{k}) | V_{ji}^{-1}(\mathbf{k})$ ], the new connection matrix is related to the Berry connection matrix through the Leibniz rule:

$$\mathcal{A}'_a(\mathbf{k}) = V^{-1}(\mathbf{k}) \mathcal{A}_a(\mathbf{k}) V(\mathbf{k}) + i V^{-1}(\mathbf{k}) \partial_a V(\mathbf{k}). \quad (\text{S37})$$

This is indeed the rule required to be a geometric connection [34]. This transformation will guarantee the invariance of intrinsic topological and geometrical quantities for generic multi-band situations, as we will see in Sec. S7. Most importantly, the covariance enables a sum vector bundle description at EPs, which will be explained in the Sec. S8.

The covariant connection matrix satisfies well-defined geometric properties. However sometimes it requires more work to compute, since the left eigenstates are the inverse of the right eigenstates (all right eigenvectors form an invertible matrix and the biorthogonal left eigenvectors is the inverse of this matrix). One may ask if there are situations where we only need to find out right eigenstates. Simplification happens when all gauge transformations can be reduced from general linear groups to unitary  $U(N)$  or orthogonal  $O(N)$  groups. A particular example is that the bands we study are spectrally isolated from each other [23, 43]. There the gauge transformation is reduced to a diagonal unitary or orthogonal matrix. We can use the following *Hermitian “connection” matrix* to capture topological properties under this condition:

$$A_a^{ij}(\mathbf{k}) = i \langle \tilde{\psi}_i(\mathbf{k}) | \partial_a \psi_j(\mathbf{k}) \rangle, \quad (\text{S38})$$

where now  $\langle \tilde{\psi}_j(\mathbf{k}) |$  is just the complex conjugate of  $|\psi_j(\mathbf{k})\rangle$  and the states are normalized according to  $\langle \tilde{\psi}_j(\mathbf{k}) | \psi_j(\mathbf{k}) \rangle = 1$ . Since the operator  $i \partial_a$  is Hermitian, the quantity  $A_a^{ij}$  is also an Hermitian matrix.

Under a change of basis  $|\psi'_j(\mathbf{k})\rangle = \sum_i |\psi_i(\mathbf{k})\rangle V_{ij}(\mathbf{k})$ , the matrix  $A_a^{ij}$  transforms as

$$A'_a(\mathbf{k}) = V^\dagger(\mathbf{k}) A_a(\mathbf{k}) V(\mathbf{k}) + i V^\dagger(\mathbf{k}) \partial_a V(\mathbf{k}). \quad (\text{S39})$$

The above transformation is not covariant for generic linear transformations, but is so for  $V \in U(N)$  or  $V \in O(N)$  since for these matrices  $V^\dagger = V^{-1}$ . Hence if we study systems where only unitary or orthogonal gauge transformations on the eigenstates are involved, the Hermitian “connection” matrix is also a well-defined geometric quantity. This is the situation when the system itself is Hermitian, or each band studied does not braid with or cross other bands via EPs.

To conclude, the Hermitian “connection” is applicable when studying the topology of bands without braidings or EPs, which is the situation of the 3-band models in the main text. However, for generic multi-band systems, albeit being easier to compute, the Hermitian “connection” matrix does not have an elegant geometric meaning as in Eq. (S35). Moreover, if we want to study the total topology of several bands meeting at an EP or bands braiding together, we must perform gauge transformations beyond the orthogonal and the unitary groups. The Hermitian “connection” matrix does not correspond to a geometric connection in these cases. This is why we use quotation marks “connection”. Nevertheless, since

$A_a^{ij}(\mathbf{k})$  has the merit of being Hermitian, it may have more physical relevance when talking about measurable quantities. We leave these discussions to future.

### S7. non-Abelian Berry curvature and topological invariants

Euler number and Chern number are the most interesting topological invariants in geometry as they can be given by integral of geometric quantities, i.e., through de Rham cohomology. The key ingredients are the invariant polynomials of curvature matrices.

With a given connection matrix, the curvature matrix is given by:

$$\mathcal{B}^{ij} = \partial_x \mathcal{A}_y^{ij} - \partial_y \mathcal{A}_x^{ij} - i[\mathcal{A}_x, \mathcal{A}_y]^{ij}, \quad (\text{S40})$$

where the last term is the commutator of the connection matrix. If we are choosing the covariant Berry connection in this formula, the corresponding Berry curvature matrix is also covariant under a change of basis:

$$\mathcal{B}(\mathbf{k}) \rightarrow V^{-1}(\mathbf{k})\mathcal{B}(\mathbf{k})V(\mathbf{k}) \quad (\text{S41})$$

The Euler number and Chern number are computed according to the scheme in Refs. 20 and 23. Chern classes correspond to  $\text{GL}_N(\mathbb{C})$ -invariant polynomials of the curvature matrix [34]. So the general linear gauge transformations in non-Hermitian systems are automatically included in computation of Hermitian number. Using the covariant Berry curvature matrix, the Chern number is given by [23]:

$$C = \int \frac{1}{2\pi} \text{tr} \mathcal{B}(\mathbf{k}) d^2k, \quad (\text{S42})$$

where the trace is taken with respect to the bands studied. Notice that due to the covariance Eq. (S41), the above equation is independent of gauge choice, as required of being a topological number.

As discussed in Sec. (S6), if the gauge transformation of the non-Hermitian system can be reduced to unitary groups, the Hermitian connection matrix is also a well defined quantity. We may similarly define an Hermitian Berry curvature and its transformation rule is given by

$$\mathcal{B}^{ij} = \partial_x \mathcal{A}_y^{ij} - \partial_y \mathcal{A}_x^{ij} - i[\mathcal{A}_x, \mathcal{A}_y]^{ij}, \quad (\text{S43})$$

$$\mathcal{B}(\mathbf{k}) \rightarrow V^\dagger(\mathbf{k})\mathcal{B}(\mathbf{k})V(\mathbf{k}) \quad (\text{S44})$$

The above equation is only covariant for  $V(\mathbf{k}) \in \text{U}(N)$ . Specific to our 3-band models, since each of the Chern band is spectrally separated from other bands, the gauge transformations can be reduced to  $\text{U}(1)$  transformations. So their Chern numbers are given by the integral of the Hermitian Berry curvature as well [23, 43]. This greatly simplifies the calculations and the measurements.

The Euler class is a  $\text{SO}(N)$ -invariant polynomial [not  $\text{GL}_N(\mathbb{R})$ -invariant] in the curvature matrix. In the non-Hermitian settings, it will require more orthonormalization procedures to be obtained from integrals of curvature. Readers with more interests may check Ref. 23. The Euler number

exists when the vector bundle is real and orientable. In this situation, the curvature matrix of a metric-compatible connection under an orthonormal basis is skew-symmetric. The Euler form is the Pfaffian of this matrix. Specific to two Euler bands in 2D systems, this is the off-diagonal component of the Berry curvature

$$\chi = \int \frac{1}{2\pi i} B^{12}(\mathbf{k}) d^2k. \quad (\text{S45})$$

One may verify the above expression is indeed invariant under a  $\text{SO}(2)$  gauge transformation on bands 1 and 2. As we are studying Hermitian Euler bands, we simply use the Hermitian Berry curvature here.

There are some cautions in choosing the wave function gauge for the Euler form. The Euler form is the off-diagonal elements of the non-Abelian Berry curvature. Under a gauge transformation  $|\psi_1\rangle \rightarrow |\psi_1\rangle, |\psi_2\rangle \rightarrow -|\psi_2\rangle$ , the off-diagonal Berry curvature changes its sign. This simply reflects that the Euler form is not invariant under  $\text{O}(2)$  transformations that include a mirror reflection. Although the Euler number is topologically quantized, the integral Eq. (S45) is equal to it only if we choose a consistent  $\text{SO}(2)$  gauge over the BZ. The gauge is chosen following Ref. 20. There are even number of Dirac nodes inside the BZ (double the Euler number), we pairwise connect them via Dirac strings (this is to say we draw lines to pair them in the BZ). Outside the Dirac strings, the wave functions  $|\psi_1(\mathbf{k})\rangle$  and  $|\psi_2(\mathbf{k})\rangle$  can be written down continuously. And when we cross a Dirac string, we let the wave function different by a gauge transformation  $|\psi_1\rangle \rightarrow -|\psi_1\rangle, |\psi_2\rangle \rightarrow -|\psi_2\rangle$ . This will respect the topology of the Dirac nodes, going around which the wave function flips its sign. Under this gauge choice, although the wave function is not continuous throughout the BZ, the Euler form is. Then the integral of the Euler form gives the correct Euler number.

The discrete numerical evaluation of the Euler number, together with the Chern number in the main text are done with the methods from Ref. 36.

### S8. Singularities of quantum geometry near EPs

We are going to discuss the covariant (non-Abelian) curvature near EPs. We focus on the EPs where two bands cross. Although the vector bundles spanned by the two eigenvectors are smooth, the covariant Berry curvature matrix under the eigenbasis can often be singular. The reason is that the transformation from a smooth basis of the vector bundles to the eigenbasis is always singular near EPs, because of eigenvector coalescence.

Let us understand this singularity. We go back to the definition of the Berry connection. We have two bands crossing each other through an EP. Without loss of generality, we denote them as band 1 and band 2. For our question, these two relevant band eigenvectors form a bundle  $F$ , which is a subbundle of the trivial vector bundle  $\text{BZ} \times \mathbb{R}^N$ . In order to look at the geometric connection  $\nabla^F$  on  $F$ , we need to project the summation of  $|\psi_{j'}\rangle$  in Eq. (S35) to span  $\{|\psi_1\rangle, |\psi_2\rangle\}$ , i.e.,

restricting the summation to  $j' = 1, 2$  [23]. The geometric meaning of Eq. (S35) is very simple, it tells us that the connection is defined to take the directional derivative by comparing the vectors in the trivial bundle  $\text{BZ} \times \mathbb{R}^N$ . In the trivial bundle, the vector space does not rotate or stretch with respect to the base manifold and thus comparison of vectors is unambiguous. When restricted to the subbundle  $F$ , the connection  $\nabla^F$  is the projection of the directional derivative in  $\text{BZ} \times \mathbb{R}^N$  to  $F$ . We can thus rewrite the projected connection  $\nabla^F$  in a more basis-independent form:

$$\Gamma(T\text{BZ}) \times \Gamma(F) \rightarrow \Gamma(F) : \nabla_{\mathbf{k}}^F v(\mathbf{k}) = P_{\text{sum}}(\mathbf{k}) \partial_{\mathbf{k}\iota} [v(\mathbf{k})], \quad (\text{S46})$$

where  $\iota$  is induced by the inclusion map  $F \rightarrow \text{BZ} \times \mathbb{R}^N$  and  $\iota(v)$  therefore can be simply written as  $v(\mathbf{k}) \in \mathbb{R}^N$  due to the trivial bundle structure. The symbol  $\Gamma(\cdot)$  means sections of a vector bundle (they are vector fields along the BZ) and  $T\text{BZ}$  represents the tangent bundle of the BZ. The inclusion map and the projection satisfy  $P_{\text{sum}} \circ \iota = id_F$ , where  $id_F$  is the identity map on  $F$ .

From this definition, the geometric connection (not the connection matrix) does not depend on which basis we choose for  $F$ . The section  $v$  in Eq. (S46) can be chosen to be any vector field on  $F$  besides the eigenvectors. This independence is also reflected by directly calculating the connection matrix under another basis. Using a linear transformation on  $|\psi_1\rangle, |\psi_2\rangle$ , we can verify that Eq. (S37) indeed agrees with Eq. (S46).

From what we showed in Sec. S4, the operator  $P_{\text{sum}}$  is continuous at EPs while  $\iota$  is always continuous. So all operations in Eq. (S46) are continuous at EPs. The geometric con-

nection for the vector bundle spanned by  $|\psi_1\rangle, |\psi_2\rangle$  is therefore continuous. From the discussion in the last paragraph, there exists a smooth basis  $v_1(\mathbf{k}), v_2(\mathbf{k})$  spanning the fibers (vector spaces) of  $F$  in the neighbourhood of the EP. The  $2 \times 2$  Berry connection matrix  $\mathcal{B}_v(\mathbf{k})$  under this basis is continuous. As we have shown in Sec. S7, the covariant curvature matrix transforms as  $V^{-1} \mathcal{B}_v V$  under a change of basis. Because the eigenvectors  $|\psi_1\rangle, |\psi_2\rangle$  coalesce near the EP, their transformation  $V(\mathbf{k})$  from the smooth basis  $v_1, v_2$  is not invertible at the EP. As a consequence, the matrix  $V^{-1}(\mathbf{k})$  diverges. This leads to a singularity of the curvature matrix under eigenbasis. A more straightforward understanding is that the biorthogonal left eigenvectors must diverge near the EP if the right eigenvectors are chosen to be continuous. However, the true underlying geometric connection of the sum bundle  $F$  is still continuous. The singularity only reflects the fact that the eigenvectors are not a good basis for the vector space they span when approaching EPs.

We see that the singularity of curvature matrix is only an artifact from the divergence of linear transformations to eigenvectors near EPs. The geometric connection and curvature themselves are continuous. This discussion also justifies why we need to employ the covariant curvature matrix when studying the overall topological structure of multiple bands meeting at an EP, as a divergent  $\text{GL}(\mathbb{C})$  or  $\text{GL}(\mathbb{R})$  transformation will restore the continuity. In the end of this section, we remark that only the sum bundle  $F$  is continuous at the EP, while the individual line bundle of each band is intrinsically singular at the EP. This is also seen as we cannot define the individual projection  $P_1$  or  $P_2$  via Eq. (S19) when  $\omega_1 = \omega_2$ . Only their sum  $P_{\text{sum}}$  is a meaningful quantity.